TREBALL FI DE GRAU

MODELING AND CONTROL OF AN ELECTRIC VEHICLE

GRAU EN TECNOLOGIES INDUSTRIALS

Author: Gerard Sabarich Mir

Director: Daniel Montesinos Miracle

Date: June 21, 2020

Location: Barcelona

ABSTRACT

Following the rising demand for electric vehicles to fight the increasing factors of pollution in urban areas, electric mobility is becoming more and more important in the automotive industry. Therefore, this study is conducted to better understand the dynamics and components of electric vehicles.

First, a theoretical study on vehicle dynamics is conducted, in which equations describing the vehicle behavior are proposed. Furthermore, analysis of energy storage, propulsion system, and less complex subsystems of the vehicle are carried out, from these analyses a model will be developed. This full vehicle model and the control system designed for it are later used to extract information on vehicle behavior and performance verification for the given car components.

Second, a more complex model is developed for the road-tire interaction, which introduces the possibility of wheel spin to appear, requiring a traction controller, based on maximum transmittable torque estimation, MTTE. The MTTE controller limits the torque provided to the wheel to prevent instabilities in the vehicle and maximizing its performance. Some issues where encountered since it works for only given torque profiles.

For the implementation of the full model, the energetic macroscopic representation, EMR, has been used, since it provides a clear interpretation of actions and reactions in each subsystem. As for the controller an inversion-based controller, IBC, is proposed to maximize control performance. The implementation of the model and control system has been carried out in Simulink.

CONTENTS

INTRODUCTION **8**

1 VEHICLE FUNDAMENTALS **10**

1.1 VEHICLE DYNAMICS 10

1.2 TIRE-ROAD INTERACTION 15

1.3 PROPULSION SYSTEM 17

1.4 ENERGY STORAGE 19

2 VEHICLE MODELLING **21**

2.1 INTRODUCTION 21

2.2 ELECTRIC VEHICLE MODEL 23

3 VEHICLE CONTROL **29**

3.1 INTRODUCTION 29

3.2 ELECTRIC VEHICLE CONTROLLER 31

4 SIMULATION **39**

4.1 FULL VEHICLE SIMULATION 40

4.2 TIRE-ROAD INTERACTION SIMULATION 48

5 PLANNING AND BUDGET **52**

5.1 PLANNING 52

5.2 BUDGET 53

6 ENVIRONMENTAL IMPACT **55**

7 CONCLUSIONS **56**

8 BIBLIOGRAPHY **58**

LIST OF FIGURES

FIGURE 1.1.1: FORCE DIAGRAM [1] 10
FIGURE 1.1.2: PRESSURE DISTRIBUTION [1] 11
FIGURE 1.1.3: GRAVITY EFFECT DECOMPOSITION [1] 12
FIGURE 1.1.4: TIRE DEFORMATION AND ROLLING RESISTANCE ON A HARD (A) AND SOFT (B) SURFACE [1] 12
FIGURE 1.1.5: FREE BODY DIAGRAM OF ONE WHEEL 14
FIGURE 1.2.1: CURVE PRODUCED BY THE MAGIC FORMULA [2] 16
FIGURE 1.3.1: DC MOTOR SCHEMATIC [1] 18
FIGURE 1.3.2: SERIES ARRANGEMENT EQUIVALENT CIRCUIT OF A DC MOTOR [1] 18
FIGURE 1.4.1: VOLTAGE CURVE OF A TYPICAL BATTERY [1] 19
FIGURE 1.4.2: DISCHARGE CURVE AT DIFFERENT DISCHARGE RATES [1] 20
FIGURE 2.1.1: GRAPHIC REPRESENTATION OF A REACTION INDUCED BY AN ACTION [3] 21
FIGURE 2.1.2: GRAPHIC REPRESENTATION OF BOTH GENERATOR AND RECEPTOR EMR SOURCES. [3] 22
FIGURE 2.1.3: GRAPHIC REPRESENTATION OF AN EMR ACCUMULATOR [3] 22
FIGURE 2.1.4: GRAPHIC REPRESENTATION OF AN EMR CONVERSION ELEMENT [3] 23
FIGURE 2.2.1: EMR BASED MODEL IMPLEMENTED IN SIMULINK 28
FIGURE 3.1.1: INVERSION-BASED CONTROL GENERAL SYSTEM REPRESENTATION [3] 29
FIGURE 3.1.2: TIME-INDEPENDENT INVERSION CONTROL, (LEFT) SINGLE INPUT, (RIGHT) MÚLTIPLE INPUT [3] 30
FIGURE 3.1.3: TIME-DEPENDENT INVERSION CONTROL [3] 31
FIGURE 3.2.1: SPEED SIGNAL FOR A STEP INPUT, (TOP) T_R=0.01 S AND (BOTTOM) T_R=0.1 S 33
FIGURE 3.2.2: $K_{XY,BRAKE}$ CALCULATOR SYSTEM 35
FIGURE 3.2.3: VOLTAGE SIGNAL FOR A STEP INPUT, (TOP) T_R=0.001 S AND (BOTTOM) T_R=0.01 S 37
FIGURE 3.2.4: IBC MODEL IMPLEMENTED IN SIMULINK 38
FIGURE 4.1.1: REFERENCE SPEED AND VEHICLE SPEED FOR A STEP INPUT 41
FIGURE 4.1.2: FORCE REFERENCE VS.OUTPUTED FORCE 41
FIGURE 4.1.3: MAXIMUM TRACTIVE EFFORT VS TRACTIVE EFFORT: (LEFT) FRONT WHEELS, (RIGHT) REAR WHEELS 42
FIGURE 4.1.4: SPEED PROFILE, REFERENCE VS. OUTPUT 42
FIGURE 4.1.5: PERCENTAGE OF BRAKING EFFORT PROVIDED BY THE MECHANIC BRAKE 43
FIGURE 4.1.6: MAXIMUM TRACTIVE EFFORT VS TRACTIVE EFFORT: (LEFT) FRONT WHEELS, (RIGHT) REAR WHEELS 43
FIGURE 4.1.7: BATTERY CURRENT AND SOC 44
FIGURE 4.1.8: REFERENCE SPEED PROFILE OF 4 NEDC CYCLE CONCATENATED 45
FIGURE 4.1.9: OUTPUT PEED PROFILE OF 4 NEDC CYCLE CONCATENATED 46
FIGURE 4.1.10: BATTERY EVOLUTION FOR A NS=160 AND NP=100 PACK 47
FIGURE 4.1.11: BATTERY EVOLUTION FOR A NS=120 AND NP=10 PACK 47
FIGURE 4.2.1: SLIP (Λ), TOP, AND FRICTION COEFFICIENT (μ), BOTTOM, FOR A CONSTANT SURFACE 48
FIGURE 4.2.2: REFERENCE TOQUE, MAXIMUM TORQUE AND CAPED REFERENCE TORQUE FOR A CONSTANT SURFACE 49

FIGURE 4.2.3: RATIO OF ACCELERATION FOR A CONSTANT SURFACE 49
FIGURE 4.2.4: SLIP (λ), TOP, AND FRICTION COEFFICIENT (μ), BOTTOM, FOR A CHANGING SURFACE..... 50
FIGURE 4.2.5: REFERENCE TOQUE, MAXIMUM TORQUE AND CAPED REFERENCE TORQUE FOR A CHANGING SURFACE 51
FIGURE 4.2.6: RATIO OF ACCELERATION FOR A CHANGING SURFACE 51
FIGURE 5.1.1: GANTT DIAGRAM OF THE PROJECT 53

LIST OF TABLES

TABLE 1.1: ROLLING RESISTANCE COEFFICIENTS [1] 13
TABLE 1.2: BURCKHARDT TIRE MODEL PARÀMETRES 16
TABLE 2.1: BATTERY CELL PARAMETERS [4] 24
TABLE 4.1: SIMULATION PARAMETERS 40
TABLE 5.1: ECONOMIC EVALUATION 54

GLOSSARY

Symbols

A_f Frontal area

A_{ev} Track

C_D Drag coefficient

F_w Aerodynamic resistance

F_g Grading resistance

F_r Rolling resistance

F_{xyx} Tractive effort

h_g Center of gravity height

J_w Road grading

L_a DC motor inductance

L Wheelbase

$Long_a$ Front-wheel distance to the center of gravity

$Long_b$ Rear-wheel distance to the center of gravity

M_{ev} Vehicle mass

N_{xy} Normal force

R_a Equivalent resistance of the DC motor

r_{curv} Turning radius

r_w Effective wheel radius

v_{ev} Linear speed of the vehicle

v_x Linear speed of the wheel center

v_w Equivalent linear speed of the wheel angular speed

Greek symbols

ω_w Angular velocity of the wheel

α Road grading

α_{xy} Duty cycle

ρ Air density

Superscript

$*$ Reference value

Subscript

bat Battery value

ev Electric vehicle value

fl Front-left wheel value

fr Front-right wheel value

m Motor value

max Maximum value

ref Reference value

rl Rear-left wheel value

rr Rear-right wheel value

$trans$ Transmission value

w Wheel value

xy General wheel value

Acronyms

SOC State Of Charge

DC Direct Current

PI Proportional Integral

EMR Energetic Macroscopic Representation

IBC Inversion Based Control

$MTTE$ Maximum Transmittable Torque Estimator

INTRODUCTION

The following project has the aim of studying the dynamic behavior of a vehicle, its battery behavior through discharge, and the capabilities of the propulsion system, as well as other internal parameters of the electric vehicle.

Once the study is done, it is proposed to develop a model of the previous subsystems studied, using the energetic macroscopic representation to visualize the actions and reactions of each subsystem more easily. Then, an inversion-based control system will be proposed so the model behaves as desired.

This controlled model, implemented in Matlab Simulink, will allow for dynamic behavior analysis as different simulations are carried out, aiming to determine the required vehicle components, such as a more powerful motor or a higher capacity battery, to fulfill a commanded speed profile.

Furthermore, a more complex model will be developed, in which the wheel slip is considered, thus a more complex control system will be required to prevent the wheel from spinning freely and control the car performance.

Objectives of the project

- General objective: Propose a model for an electric vehicle based on IMR, the required IBC control system and analyze the dynamic and electric behavior of the electric vehicle.
- Specific objectives:
  - Study the dynamic behavior of a vehicle as it interacts with the environment.
  - Study the relation between tire slip and friction force.
  - Study the propulsion system and battery of the vehicle
  - Model vehicle behavior and implement it in Simulink.
  - Design an IBC control system for the modeled vehicle and implement it in Simulink.
  - Analyze the dynamic and electric behavior of various subsystems of the vehicle.

Scope of the project

The project includes:

- The theoretic study of the dynamic behavior of an electric vehicle.
- The theoretic study of the tire-ground relation and its ideal controller.

- The ideal model of the full vehicle.
- The reduced model for the tire-ground interaction.
- The control system for the vehicle.
- The traction control for the reduced model.

1 VEHICLE FUNDAMENTALS

1.1 VEHICLE DYNAMICS

As any object moving through a fluid and in contact with a road, a vehicle is subjected to external forces, such as drag produced by contact with the given fluid, or gravity pushing the object downwards. Therefore, a tractive effort must overcome these external forces, to propel the object forward, this is represented by

$$\frac{dv}{dt} = \frac{\Sigma F_t - \Sigma F_{tr}}{M}, \tag{1}$$

where dv/dt is the vehicle acceleration, M is the vehicle mass, $\sum F_t$ is the sum of all tractive efforts, and last, $\sum F_{tr}$ is the sum of the resistive forces. These are represented in Figure 1.1.1.

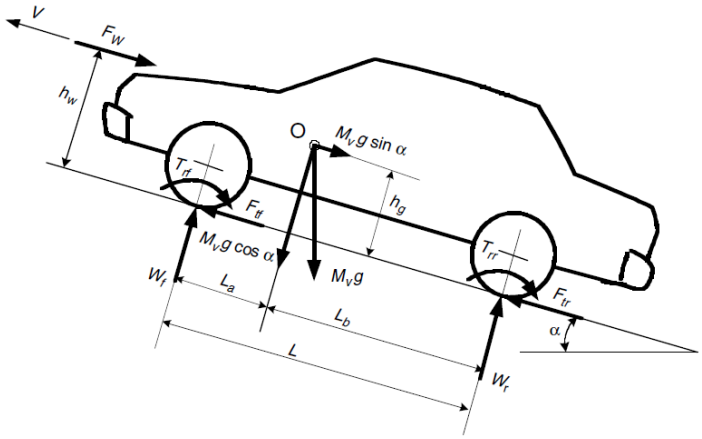

Figure 1.1.1: Force Diagram [1]

1.1.1 Resistances

The sum of the resistive forces can be divided into three, aerodynamic drag, rolling resistance, and grading resistance, these are introduced below.

- **Aerodynamic drag**

Drag is created by high-pressure areas in front of the EV and low-pressure areas in the back. The frontal high-pressure area is created as the vehicle pushes through the air, as it cannot be displaced immediately, the air in front is compressed creating a force against the vehicle movement. As for the rear low-pressure area, following the same principle, the air cannot fill the

empty space immediately, therefore creating a depression pulling the vehicle backward. This phenomenon is represented in Figure 1.1.2. These two effects are combined to generate a force against the vehicle movement,

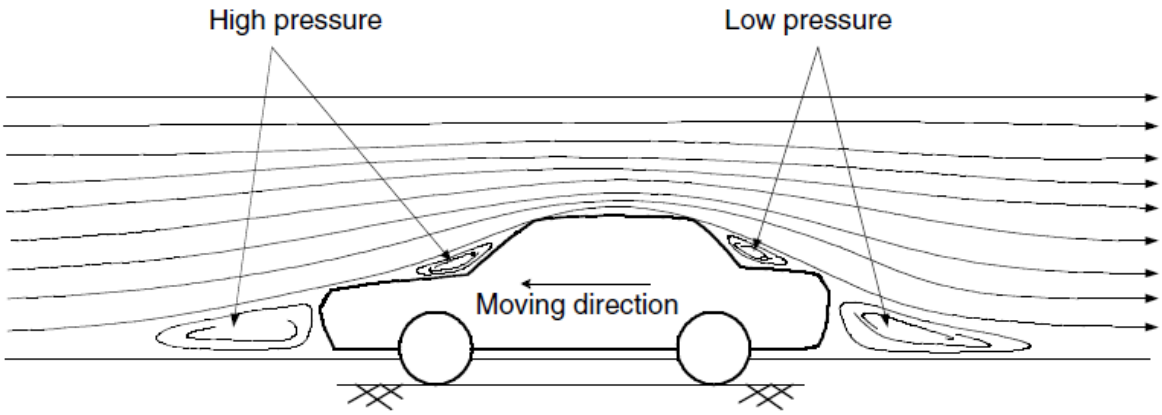

Figure 1.1.2: Pressure distribution [1]

Drag will be considered a simple force applied at a height h_w parallel and opposed to the vehicle movement, as represented in Figure 1.1.1. As a simplification, on a road car, h_w can be assumed to be equal to h_g.

The equivalent force provided by air resistance is described as

$$F_w = \frac{1}{2}\rho A_f C_d (v - v_w)^2, \tag{2}$$

where ρ is the air density, A_f is the frontal area of the vehicle, C_d is the aerodynamic drag coefficient, v is the vehicle velocity and v_w is the wind velocity, this last one will be considered 0 throughout the project.

- **Grading Resistance**

As gravity pushes downwards on the vehicle, two forces are generated, a force pushing the vehicle into the ground and, in case there is a slope, a force along the road slope always pointing downwards, as shown in both Figures 1.1.1 and 1.1.3. This later force is the grading resistance, it is described as

$$F_g = M_v g \sin\alpha, \tag{3}$$

where g is the gravitational acceleration and α is the grading slope. It must be stated that grade slope α is only valid for small road angles since the following simplification is being made:

$$i = \frac{H}{L} = \tan\alpha \approx \sin\alpha, \tag{4}$$

where H is the height cleared each L distance, as represented in Figure 1.1.3.

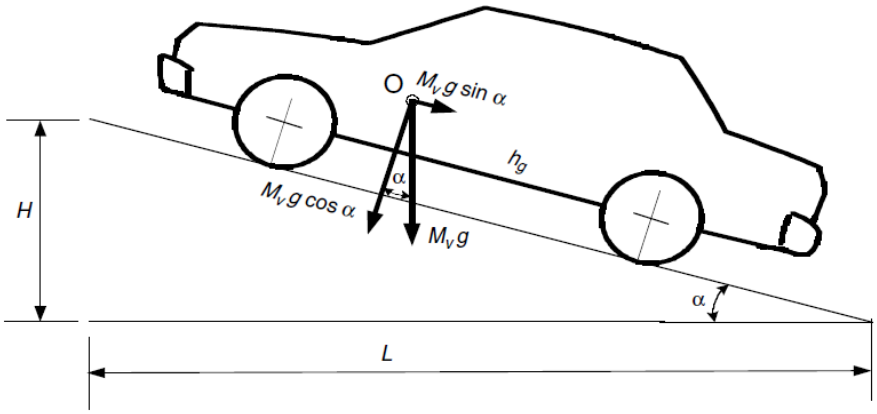

Figure 1.1.3: Gravity effect decomposition [1]

- **Rolling resistance**

As the tires deform while in contact with the ground, an asymmetry is generated in the pressure distribution underneath the contact patch, due to the material accumulation in front of the wheel, and lag of it in the rear. This creates a not centered equivalent force, which in turn generates a torque against the wheel movement, shown in Figure 1.1.4.

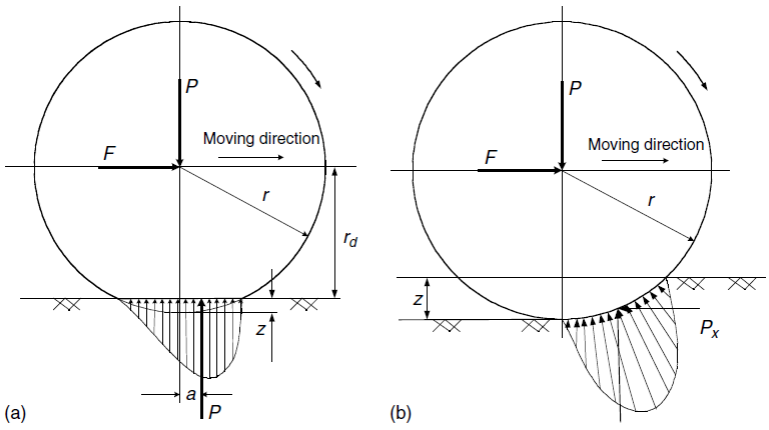

Figure 1.1.4: Tire deformation and rolling resistance on a hard (a) and soft (b) surface [1]

The moment generated can be described as

$$T_r = Pa, \tag{5}$$

where P is the normal load generated by gravity. If the torque is translated to a force, it can be stated that

$$F_r = P f_r \cos\alpha, \tag{6}$$

where f_r is the rolling resistance coefficient. This rolling resistance coefficient is a function of many road-tire variables which makes it difficult to calculate, therefore a table with the main values in some situations is proposed in Table 1.1.

Conditions	Rolling resistance coefficient
Car tires on concrete or asphalt	0.013
Car tires on rolled gravel	0.02
Tarmac	0.025
Unpaved road	0.05
Field	0.1–0.35
Truck tires on concrete or asphalt	0.006–0.01
Wheels on rail	0.001–0.002

Table 1.1: Rolling resistance coefficients [1]

1.1.2 Dynamic equation

As a reduced version was introduced in (1), and the resistive forces have been presented, an extended version

$$M_v \frac{dV}{dt} = \left(F_{frt} + F_{rrt} + F_{flt} + F_{rlt}\right) - \left(F_r + F_w + F_g\right), \tag{7}$$

is provided, where the tractive effort is divided into the individual contribution of each wheel. Also, the resistive forces are represented by their contribution.

The maximum tractive effort, overlooking complex tire-road interaction, can be described as

$$F_{xyt,max} = \mu N_{xy}, \tag{8}$$

where μ is the adhesion coefficient and N_{xy} is the normal load applied to each wheel. The normal load may be different at each wheel depending on the acceleration profile, the turn steepness and speed carried through the turn. Therefore, a different expression is provided for each wheel. For the front wheels and considering only longitudinal dynamics, the normal load is

$$N_{fy} = \frac{L_b}{L} M_v g cos(\alpha) - \frac{h_g}{L}\left(F_w + F_g + M_v g f_r \frac{r_w}{h_g}\cos(\alpha) + M_v \frac{dv}{dt}\right), \tag{9}$$

and for the rear wheels

$$N_{fy} = \frac{L_a}{L} M_v g cos(\alpha) + \frac{h_g}{L}\left(F_w + F_g + M_v g f_r \frac{r_w}{h_g}\cos(\alpha) + M_v \frac{dv}{dt}\right), \quad (10)$$

For the lateral component, taking the curvature, but overlooking the stirring angle effects and lateral slip force. The expressions are

$$N_{xl} = N_{xy} + \frac{M_v v^2 h_g}{r_{curv.} A_{ev}}, \quad (11)$$

for the left wheels, and

$$N_{xr} = N_{xy} - \frac{M_v v^2 h_g}{r_{curv.} A_{ev}}, \quad (12)$$

for the right ones. Where r_{curv} is the radius of the turn, being positive for left turns and positive for right turns, and A_{ev} is the track of the vehicle, distance from wheel to wheel.

1.1.3 Wheel dynamics

As the resistive forces and dynamic equations have been discussed, all the parameters from (1) have been introduced but the tractive force. This one will be dictated by the interaction between the ground and tire. Before describing the mentioned interaction, an introduction to tire dynamics is due.

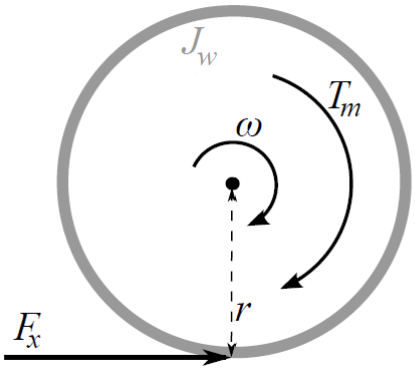

Figure 1.1.5: Free body diagram of one wheel

The dynamic of the wheel is described by the toque balance

$$J_w \frac{d\omega}{dt} = T_m - F_x r, \quad (13)$$

where J_w is the wheel inertia, ω is the rotating speed, T_m is the torque provided by the motor, r is the radius of the wheel and F_x is the friction force acting on the wheel, represented in Figure 1.1.5. F_x is defined as

$$F_x = \mu(\lambda)N, \tag{14}$$

where N is the normal load, and μ is the friction coefficient, which is not assumed constant, it will be defined as a complex function of slip (λ). In the following chapter different approaches and solutions to the mentioned function are presented.

1.2 TIRE-ROAD INTERACTION

Before defining the relation between the friction coefficient and slip, slip must be defined, and it is done in [2] as

$$\lambda = \frac{v_\omega - v_x}{v_\omega}, \tag{15}$$

$$v_\omega = r_w\omega, \tag{16}$$

where λ is the slip and v_x is the linear speed of the wheel. This description is only valid for an acceleration profile; therefore, a modification is proposed, described as

$$\lambda = \frac{v_\omega - v_x}{\max(v_\omega, v_x)}. \tag{17}$$

As mentioned earlier, the interaction between tire and ground, represented by, μ is non-trivial, and several approaches have been made to define a reliable model. In this chapter two of them are discussed: Burckhardt's model (1993) and Pacejka's (2002) [2].

1.2.1 Pacejka's model

Starting by Pacejka, the expression, named the Magic Formula [2]

$$F_x = D_x \sin(C_x \arctan[B_x(1 - E_x)\cdot\lambda_x + E_x \arctan(B_x\lambda_x)]) + S_{vx}, \tag{18}$$

where F_x is the friction force, S_{vx} is the vertical shift, B_x is the stiffness factor, C_x is the shape factor, D_x is the peak value and E_x is the curvature value. A graphic representation is provided in Figure 1.2.1.

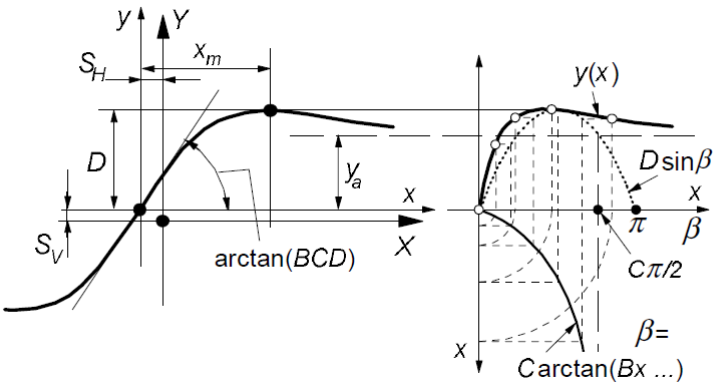

Figure 1.2.1: Curve produced by the Magic Formula [2]

The equations for the parameters are complex and may diverge depending on the vehicle, tires, or road. Therefore, given that the project aims to deliver a generic model with its controller, a simpler relation between tire and ground will be used. This simpler model is introduced below.

1.2.2 Burckhardt's model

As the Pacejka model is deemed too complex for the scope of the project since the necessary values cannot be measured, a simpler model is introduced: the Burckhardt model. The model is described by

$$\mu(\lambda) = c_1\left(1 - e^{-c_2\lambda}\right) - c_3\lambda, \tag{19}$$

where c_1 is the maximum value of the friction curve, c_2 is the friction curve shape and c_3 is the friction curve difference between the maximum value and the value at λ=1. These coefficients are represented in Table 1.2.

	C_1	C_2	C_3
Asphalt, dry	1.2801	23.99	0.52
Asphalt, wet	0.857	33.822	0.347
Concrete, dry	1.1973	25.168	0.5373
Cobblestone, dry	1.3713	6.4565	0.6691
Cobblestone, wet	0.4004	33.708	0.1204
Snow	0.1946	94.129	0.0646
Ice	0.05	306.39	0

Table 1.2: Burckhardt tire model paràmetres

The virtue of this model is its simplicity, only three parameters are required to define the relationship between the tire and ground for each surface, although, fidelity to reality will be inferior. As an example, in Pacejka's model a slight difference in the camber of the wheel may affect the curve, this difference would go unnoticed in Burckhardt's model. Moreover, the

differences between the curves are significant even for analog situations. Furthermore, the Burckhardt model does not follow properly the curvature after the peak value, providing a slight divergence from reality at slips lager than the optimal.

Given these drawbacks, it would be preferable to use the Pacejka model, but since the information required to compute its parameters is not available, the generic Burckhardt model will be enough.

1.3 PROPULSION SYSTEM

As the dynamics of a vehicle have been described, it is time to define how to provide this motion to the vehicle. The tractive effort will be provided by a motor, but there are multiple options to choose from.

Since it is an electric vehicle the limitation is clear, it must be an electric machine, but still, there is a great variety to choose from. The decision can be made considering many factors, such as power, reliability, cost, availability, or control necessities. The solutions can vary from a simple DC motor, an induction machine, or a brushless synchronous machine, to name a few, each of them more complex to control.

As the main objective is not to design a complex motor controller, the simpler motor is chosen, the DC motor. Its working principle relays on a wire carrying electrical current located inside a magnetic field, inducing a perpendicular force to both the wire and magnetic field defined by

$$T = BIL\cos\alpha, \tag{20}$$

where T is the torque produced, B is the magnetic field density, I is the current flowing through the wire, L is the wire length and α is the angle between the coil plane and magnetic field shown in Figure 1.3.1. The torque is at its maximum when the angle is equal to 0 since the cosine will equal 1. Therefore, brushes and multiple coils are used to maintain maximum and constant torque.

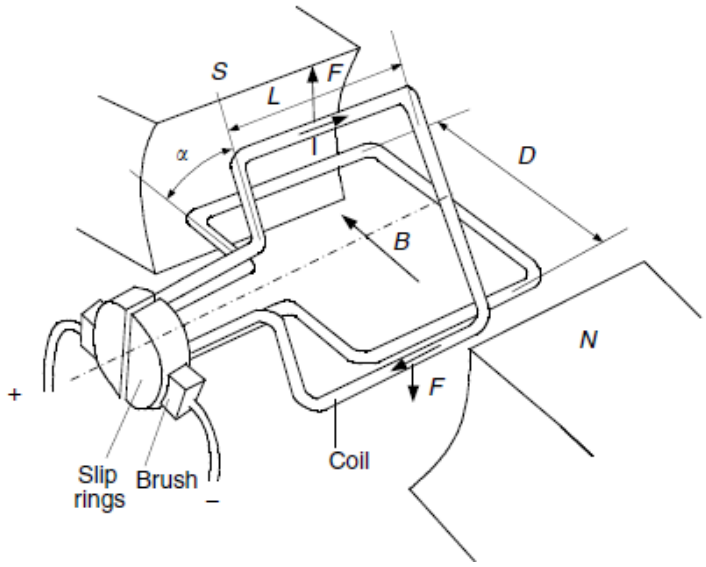

Figure 1.3.1: DC motor schematic [1]

There are multiple arrangements for DC motors depending on the mutual interconnections, but in this project, a series excitement arrangement is selected, its equivalent circuit is shown in Figure 1.3.2.

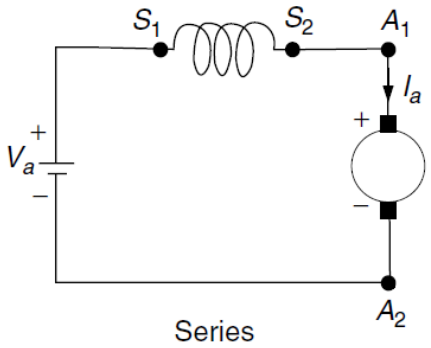

Figure 1.3.2: Series arrangement equivalent circuit of a DC motor [1]

This arrangement behavior can be described by

$$U_a = R_a i_a + L_a \frac{di_a}{dt} + E, \tag{21}$$

$$E = k\phi_f \omega, \tag{22}$$

$$T = k\phi_f I_a, \tag{23}$$

where U_a is the voltage applied to the ends of the motor, R_a is the equivalent resistance of the circuit and L_a is the inductance of the coil, E is the back electromotive force, $k\phi_f$ is the emf constant, and i_a is the current flowing through the motor.

As the equations are listed, the control problem is presented. For the motor to operate at a desired torque and speed, the voltage must be controlled, something the battery cannot do since the voltage supply is constant. Therefore, an element in between the two is required, a DC/DC converter, which will modulate the voltage fed to the motor.

1.4 ENERGY STORAGE

Once the dynamics and the propulsion have been solved, it is necessary to define the energy supplier of the vehicle, the battery. As well as the electric machine, the list of solutions for energy storage is large, therefore a brief introduction to battery theory is presented.

Fist, the first characteristic to describe is the discharge curve. As the battery empties, the voltage drops, going from the rated open-circuit voltage to the cut-off voltage, represented in Figure 1.4.1, this curve is found through testing and experimentation and is provided by the manufacturer. This curve must be monitored at all times to prevent damage to the battery, cutting the voltage supply when the cell voltage falls below the cut-off voltage.

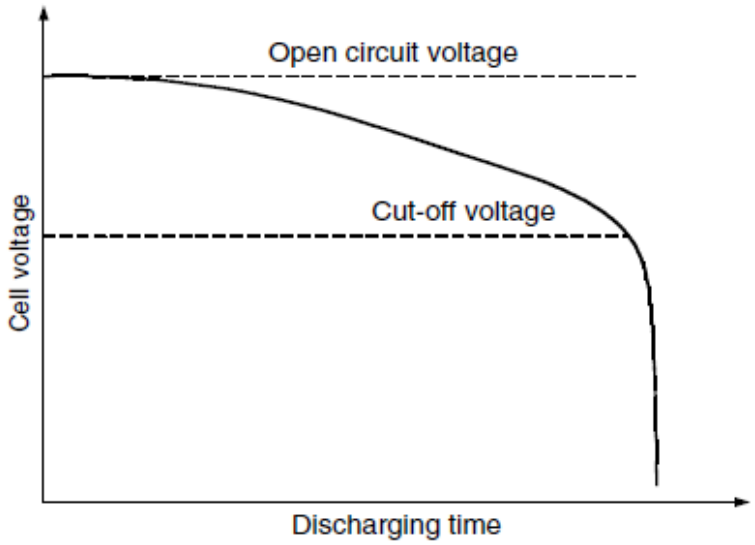

Figure 1.4.1: Voltage curve of a typical battery [1]

Second, the capacity and discharge rate are described. Capacity represents the amount of energy the battery can generate at a given discharge rate until the cut-off voltage is reached. The discharge rate represents the amount of current circulating through the battery and is represented as a fraction of the rated capacity by the discharging current, the lower it is the higher the capacity, as shown in Figure 1.4.2.

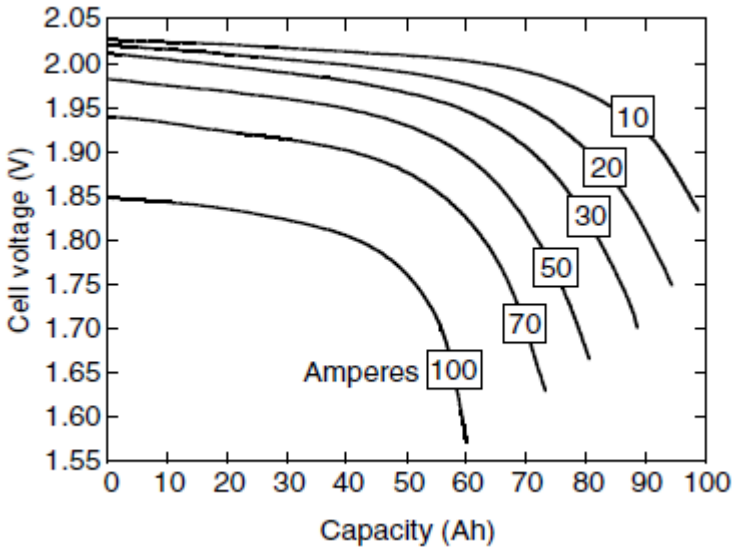

Figure 1.4.2: Discharge curve at different discharge rates [1]

At last, the state of charge is introduced, SOC for short, it is defined as the ratio of remaining capacity to the fully charged capacity. It is expressed as

$$SOC = SOC_0 - \int \frac{i\,dt}{Q(i)}, \tag{24}$$

where SOC_0 is the initial SOC, which will be Q at time 0 if the battery starts fully charged, and Q(i) is the capacity at a current rate i.

2 VEHICLE MODELLING

Once the theory behind vehicle dynamics, propulsion systems and batteries has been introduced, the next step can be taken, create a model for it.

To create a visual model, the Energetic Macroscopic Representation [3], EMR for short, is used. Therefore, a brief introduction to the chapter is provided to describe the basics of EMR.

At the end of the chapter the complete model, based on EMR and implemented in Simulink, is represented in Figure 2.2.1.

2.1 INTRODUCTION

EMR consists of a physic representation of a system with two considerations. First, every action induces a reaction, as shown in Figure 2.1.1. And second, physical causality is integral and must be respected, thus the present output of the system can depend on past inputs, but never on future ones.

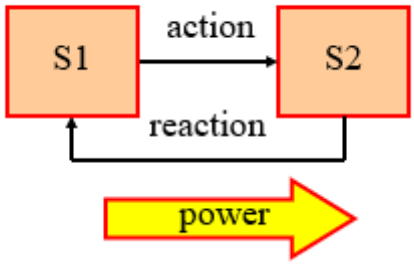

Figure 2.1.1: Graphic representation of a reaction induced by an action [3]

Once the considerations have been mentioned, it is due to introduce the elements that take part in EMR, a small description for each of them is provided.

2.1.1 Energy sources

Their purpose is to define the environment of the system, even if it is an energy generator or a receptor. An example in Figure 2.1.2.

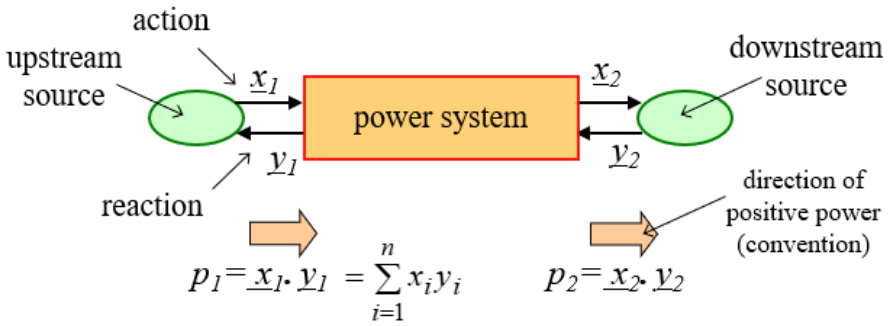

Figure 2.1.2: Graphic representation of both generator and receptor EMR sources. [3]

2.1.2 Energy storage elements

These elements are called accumulators, as the name suggests they accumulate energy, following the causality principle, and are defined by

$$\underline{y} \propto \int f(\underline{x}_1, \underline{x}_2) dt, \tag{25}$$

where $\underline{x}_1$ and $\underline{x}_2$ are the inputs in the block and $\underline{y}$ is the output, as shown in Figure 2.1.3.

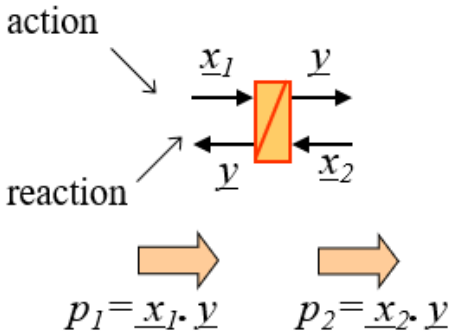

Figure 2.1.3: Graphic representation of an EMR accumulator [3]

2.1.3 Energy conversion elements

These blocks act as a gain with a slight variation, they can be controlled by a tuning input. These blocks can be monophysical or multyphysical, depending on the system requirements. The block follows the expression

$$y_2 = f(\underline{x}_1, \underline{z}), \tag{26}$$

$$y_1 = f(\underline{x}_2, \underline{z}), \tag{27}$$

where $\underline{x_1}$ and $\underline{x_2}$ are the inputs of the block, $\underline{z}$ is the tuning vector and $\underline{y}$ is the output, as shown in Figure 2.1.4.

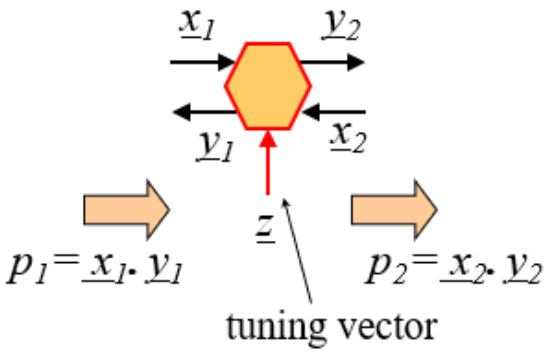

Figure 2.1.4: Graphic representation of an EMR conversion element [3]

2.1.4 Energy distribution elements

Last, the distribution elements take care of the routing of the signals, being able to divide it, or distribute it to many blocks, as well as, coupling these signals into a single block.

2.2 ELECTRIC VEHICLE MODEL

As the representation system used has been introduced, the model of the vehicle is presented.

2.2.1 Battery

As the theory and parameters have been introduced and the complex discharge curve has been presented, a model is introduced in [4], represented by

$$V_{bat} = E - Ri, \tag{28}$$

$$E = E_0 - K\frac{Q}{Q - \int idt} + Ae^{-B\int idt}, \tag{29}$$

where R is the internal resistance of a battery cell, E is the no-load voltage, E_0 is the battery constant voltage, K is the polarization voltage, Q is the battery capacity, $\int idt$ is the actual charge of the battery and A and B are experimental values related to the discharge curve.

As for the characteristic values of the discharge curve, these are different for each battery technology, therefore, parameters for a lithium-ion battery cell, used in the vehicle model, with a rated voltage of 3.6 V, a capacity of 1 Ah and a cut-off voltage of 2.5 V are provided, in Table 2.1.

E_0(V)	R(Ω)	K(V)	A(V)	B(Ah^{-1})
3.7348	0.09	0.00876	0.468	3.5294

Table 2.1: Battery cell parameters [4]

These parameters are for an individual cell, therefore, must be scaled up. This is done by connecting these cells in both series and parallel following the equations

$$V_{bat} = V_{cell} \cdot n_{series}, \tag{30}$$

$$n_{series} = \frac{V_{bat\ req.}}{V_{cell}}, \tag{31}$$

$$n_{parallel} = \frac{Q_{bat\ req.}}{Q_{cell}}, \tag{32}$$

Since running out of battery in the middle of a simulation is not desired, a greatly oversize battery is provided, one with 160 cells per row and 100 rows. Through simulation, they could be trimmed down.

2.2.2 Distributor

As the energy is generated at the battery, it must be distributed to the four DC/DC converters, one for each wheel. The voltage will be maintained as that outputted by the battery, but the current flowing towards the battery will be that of the sum of the outputted by the four DC/DC converters. This is described by

$$V_{bat} = V_{fra} = V_{rra} = V_{fla} = V_{rla}, \tag{33}$$

$$I_{bat} = I_{fra} + I_{rra} + I_{fla} + I_{rla}, \tag{34}$$

where V_{xy} is the voltage fed to the DC/DC converters and I_{xy} is the current coming from the DC/DC converters.

2.2.3 DC/DC converter

Once the energy division is done, the next blocks in line are the DC/DC converters, all of them being equal. The DC/DC converter is modeled as a monophysical conversion element with a

control input which converts the fixed DC voltage coming from the battery into the desired DC voltage required by the controller through the duty cycle. The DC/DC converter is model as

$$U_{xya} = \alpha_{xy} V_{xya}, \quad (35)$$

$$I_{xy} = \alpha_{xy} I_{xya}, \quad (36)$$

where U_{xya} is the voltage fed to the motor, I_{xya} is the current coming from the motor, and $\alpha_{xya} \in [-1,1]$is the duty cycle and is the control signal used to control the force outputted by the vehicle.

2.2.4 DC motor

At this point, a causal system is encountered, the electric conversion, in which the voltage differential at the coils of the motors induces a current through it, as described by (21) and (22). As for the electromechanical conversion, it is a non-causal system described by (23).

The values taken for the simulation are, the rated voltage as 400 V, the rated current as 89.5 A, the back electromagnetic force ($k\phi_a$) as 1.2396 Vs/rad, the equivalent resistance as 0.35 Ω and the equivalent inductance as 6.5 mH.

2.2.5 Transmission

The transmission is a simple monophysical conversion block, only in charge of applying the fixed reduction k_{gear}. It follows the equation

$$T_{xytrans} = k_{gear} T_{xym}, \quad (37)$$

$$\omega_{xym} = k_{gear} \omega_{xytrans}, \quad (38)$$

where $T_{xytrans}$ is the torque applied to the wheel and $\omega_{xytrans}$ is the angular speed induced by the wheel. For the transmission modeling, k_{gear} is taken as 5.

2.2.6 Brake distributor

As an electric vehicle can alternate between mechanic braking and regenerative braking through the electric machine. This will mean two sources of braking torque are available, that of the ideal brake and that of the motor, where the outputted torque to the wheel can be defined as

$$T_{xyw} = \mathrm{T}_{xytrans} + T_{xybrake}, \quad (39)$$

where $T_{xybrake}$ is the torque provided by the brake, which can only be negative.

2.2.7 Wheel

- **Ideal wheel**

Although the explanation on tire-road dynamics in chapter one was done with the non-linear and more complex theory, described by the Pacejka and Burckhardt models, a simpler and easier to control model is proposed to extract initial simulations.

The rigid model of an ideal wheel does not consider the slip of the tire, and understands de phenomenon as a simple conversion, just like the transmission. It follows the equation

$$F_{xyx} = \frac{T_{xytrans}}{r_w}, \tag{40}$$

$$\omega_{xyx} = \frac{v_{xyx}}{r_w}, \tag{41}$$

where v_{xyx} is the linear velocity at the center of the wheel and F_{xyx} is the force transmitted from the wheel to the chassis. For the model, the effective radius is taken as 0.26 m.

- **Non-ideal wheel**

As the linear, simpler, model is introduced, the non-linear which models the slip of the wheel is presented. It takes the same inputs and produces the same outputs but is no longer a simple converter. As inertia is considered it becomes an accumulator. Considering (13), (14), (16), (17), and (19) the model can be defined.

For the model, the total motor, transmission, and wheel inertia is taken as 0.5 kg/m^2.

2.2.8 Union

The last energy distribution element in the model, required to couple all the tractive efforts coming from the wheels and transmitting the velocity required at each wheel as a reaction. The behavior is defined as

$$F_{ev} = F_{frx} + F_{rrx} + F_{flx} + F_{rlx}, \tag{42}$$

$$v_{frx} = v_{rrx} = \frac{v_{ev}}{r_{curv}}\left(r_{curv} + \frac{A_{ev}}{2}\right), \tag{43}$$

$$v_{flx} = v_{rlx} = \frac{v_{ev}}{r_{curv}}\left(r_{curv} - \frac{A_{ev}}{2}\right). \tag{44}$$

For the model, the track (A_{ev}) of the car is taken as 1.65 m.

2.2.9 Chassis

Once the total force produced by the vehicle is computed at the union block, it is inputted into an accumulator and the vehicle speed is outputted, as described by (1) in the first chapter. Mass for the vehicle is taken as 1000 kg.

2.2.10 Environment

At last, the final block in the model, the environment, takes the vehicle speed as an input and computes the resistive forces for the given speed, as described in (2), (3), and (6), introduced in the first chapter.

For environment modeling, the following values are provided. The air density is taken as 1.22521 kg/m^3, the drag coefficient as 0.35, the frontal area as 2 m^2, and the rolling coefficient as 0.017.

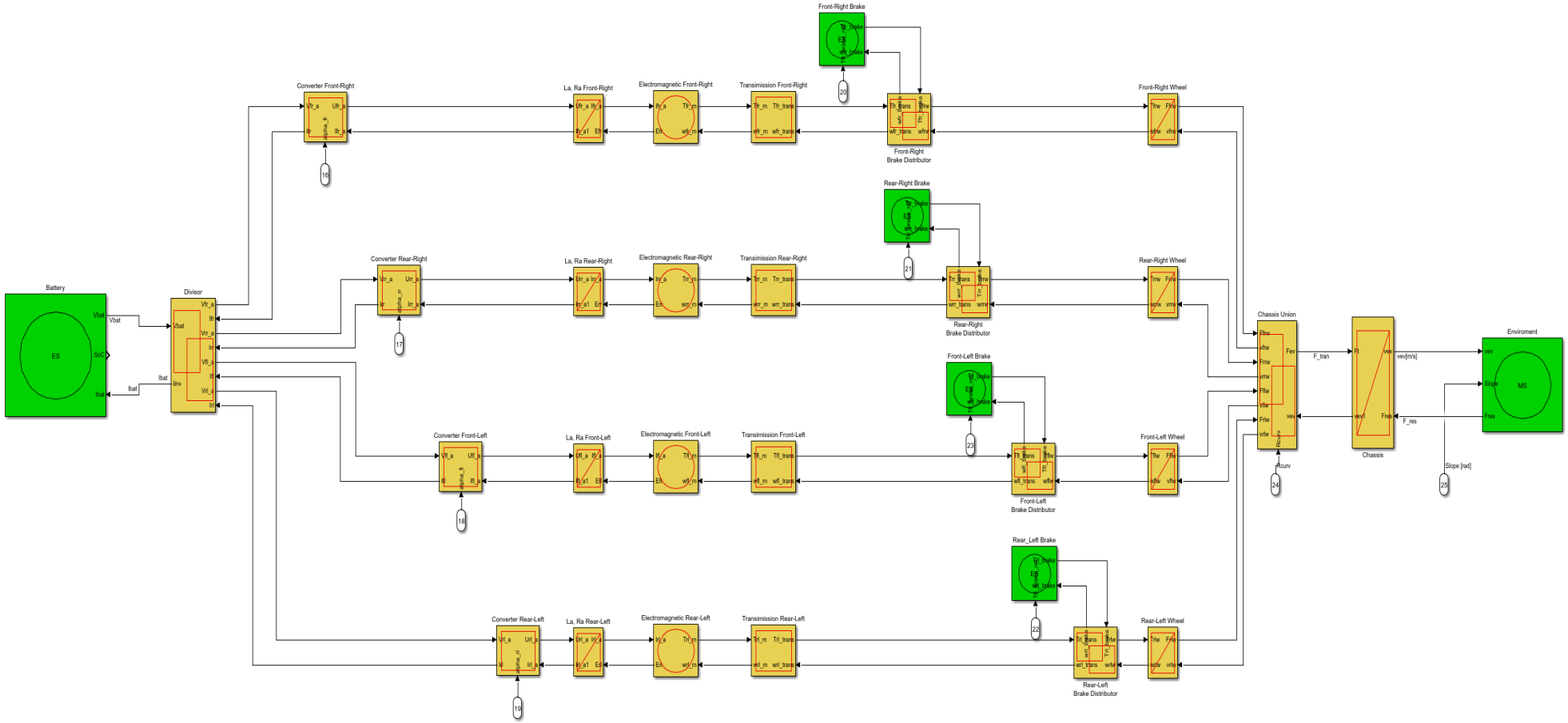

Figure 2.2.1: EMR based model implemented in Simulink

3 VEHICLE CONTROL

As the vehicle model has been described, the introduction to the control system is provided. This control system is based, in its majority, in a maximum control structure, which consists of directly inverting the model. The problem is, being a causal system, some blocks will not allow for direct inversion, therefore these will need an indirect inversion, in other words, a closed-loop controller. As it has been done for the modeling, an introduction to control theory and the control for each subsystem is described.

At the end of the chapter, the complete IBC control system implemented in Simulink is represented in Figure 3.2.4.

3.1 INTRODUCTION

The control system for the project is based on an inversion-based control, IBC for short. As the name implies, the objective is to invert the system, as shown in Figure 3.1.1 for a generic system. It can be seen the desired effect is the input to the controller, which computes the right cause required by the system which will later compute the actual output of the system. Depending on the time relationship presented by the system, the inversion will vary.

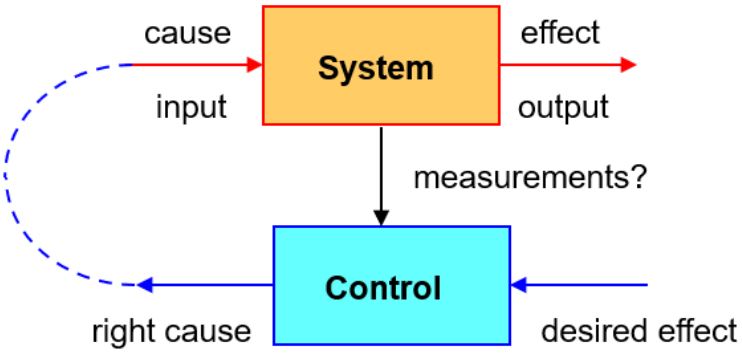

Figure 3.1.1: Inversion-based control general system representation [3]

3.1.1 Time independent relationship

Also known as non-causal systems, they accept the direct inversion of the system. This system can be a multiple-input one, although only one will be the reference, the rest must be measured values from the system itself, as shown in Figure 3.1.2.

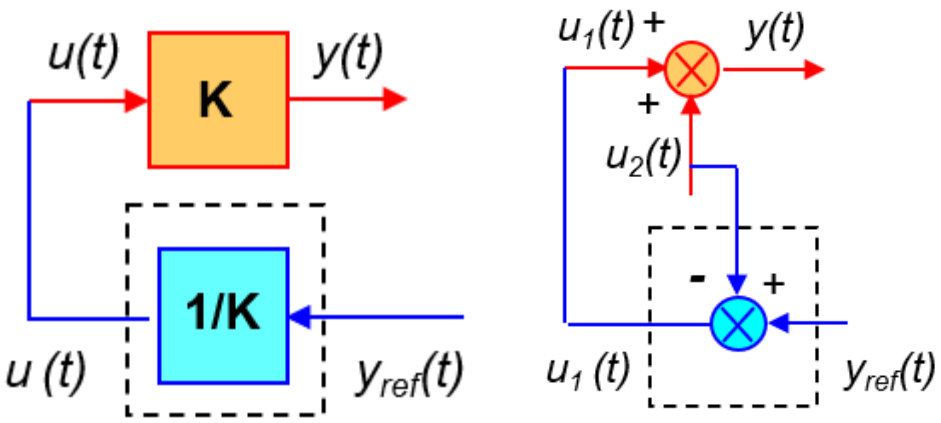

Figure 3.1.2: Time-independent inversion control, (left) single input, (right) múltiple input [3]

If the system is described by the generic expression

$$y(t) = \sum_{i=1}^{nº\ inputs} u_i(t), \tag{45}$$

where y(t) is the output value and $u_i(t)$ are the inputs. Then the direct inversion is described as

$$u_j(t) = y_{ref}(t) - \sum_{i=1}^{nº\ inputs \notin j} u_i(t), \tag{46}$$

where $u_j(y)$ is the chosen variable to act on the output y(t), $y_{ref}(t)$ is the reference input, and $u_i(t)$ are the disturbances inputs.

3.1.2 Time-dependent relationship

Also known as causal systems, and contrary to the non-causal ones, they cannot be directly inverted. Therefore, an indirect inversion mechanism, a controller, is required, as shown in Figure 3.1.3. This controller can be one of many options, but the one used for accumulative systems in the project will be a PI controller due to its simplicity and easy tuning through simulation.

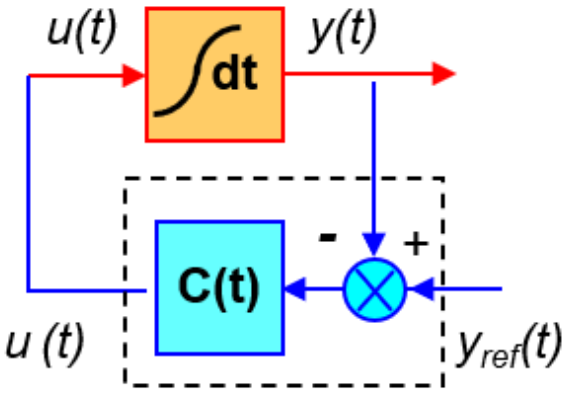

Figure 3.1.3: Time-dependent inversion control [3]

If the system is described by the generic expression

$$y(t) = \int u(t)dt, \tag{47}$$

where y(t) is the output value and u(t) is the input. Then the indirect inversion is described as

$$u(t) = C(t)\left[y_{ref}(t) - y_{meas}(t)\right], \tag{48}$$

where u(y) is the variable to act on the output y(t), y_{ref}(t) is the reference input, y_{meas}(t) is the measured output desired to control and C(t) is the controller transfer function chosen for the system.

3.2 ELECTRIC VEHICLE CONTROLLER

As the control theory has been presented the individual controllers for each presented model system, in reverse order as they were presented, as the signal flows.

3.2.1 Chassis

The system to invert, a causal system, requires an indirect inversion, through a PI controller, as mentioned before. The model is described by a first-order transfer function, defined by

$$G(s) = \frac{1}{As + B}, \tag{49}$$

where A for the chassis being the vehicle mass M and B equals 0.

The PI controller has a transfer function

$$G(s) = K_P + K_D s, \tag{50}$$

where the K_P is the proportional part of the controller and K_I is the integral part. These values are easy to compute for a first-order system from a given rise time t_r, through the α parameter defined as

$$\alpha = \frac{\ln(9)}{t_r}, \tag{51}$$

and from it, the proportional and integral constants are computed as

$$K_P = \alpha A, \tag{52}$$

$$K_I = \alpha B. \tag{53}$$

Therefore, the PI controller will only be proportional, and

$$K_P = \frac{\ln(9)}{t_r} M_{ev}, \tag{54}$$

where t_t can be adjusted as a controller performance is wanted. In Figure 3.2.1 the effect of t_r is shown, the time it takes for the output to go from 10% to 90% of the final value is t_r. The expression for the control system is represented by

$$F_{ev}^* = K_P[v_{ev}^* - v_{ev}] - F_{res}. \tag{55}$$

If a driver were in the vehicle acting on the accelerator pedal, the controller would be the driver himself and would try to behave as close as the proportional controller does.

For the measurements of v_{ev} and F_{res} estimators are used. These estimators emulate the job of sensors, if the variable is measurable, or act as estimators. For these variables, speed can be measured, but force cannot, therefore must be estimated, as it is done in the environment source block.

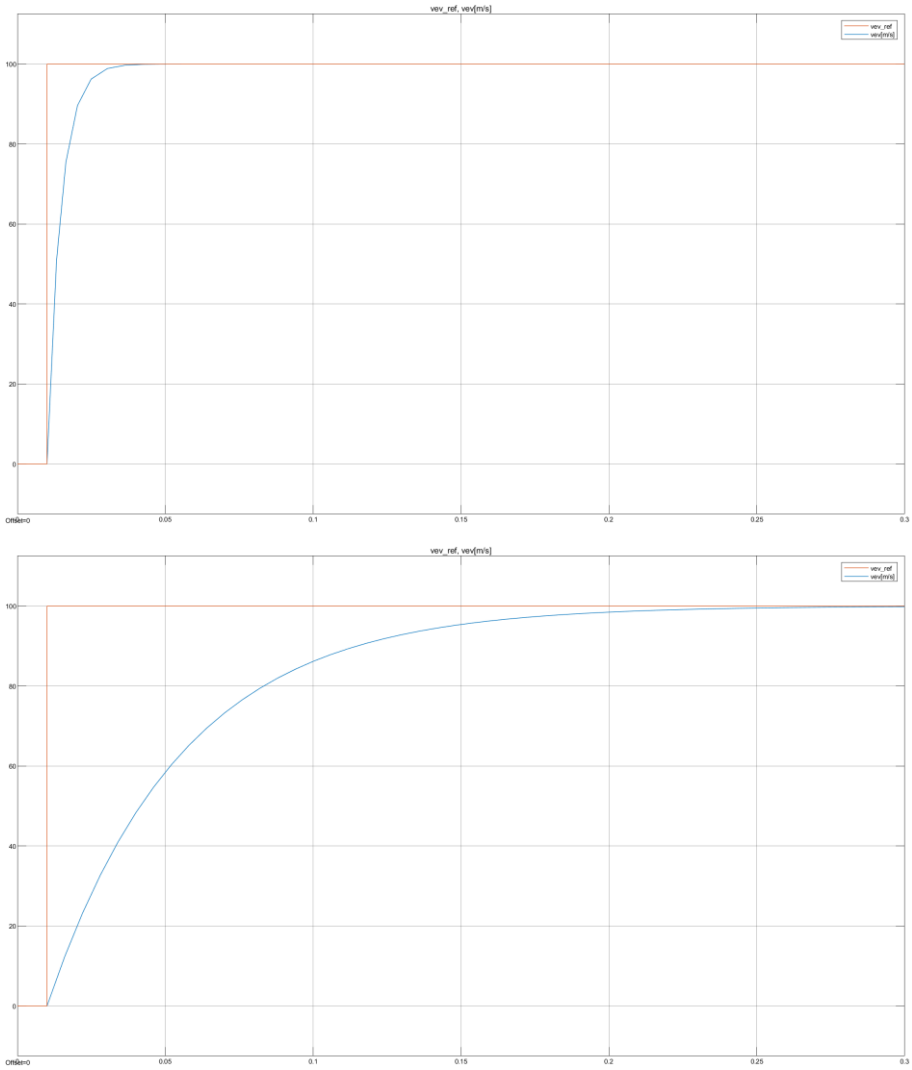

Figure 3.2.1: Speed signal for a step input, (top) t_r=0.01 s and (bottom) t_r=0.1 s

3.2.2 Union

The union block becomes a divisor when directly inverted, therefore a selector is introduced to decide how the energy is distributed. It will be treated as a rigid differential like the transmission in which the force is equally distributed to each wheel. As an addition, the reference traction force is limited according to the weight distribution at each wheel. Thus,

$$F^*_{frx} = 0.5^2 F^*_{ev}, \in \left[-F_{fr,max}, F_{fr,max}\right], \tag{56}$$

$$F^*_{rrx} = (1-0.5)0.5F^*_{ev}, \in \left[-F_{rr,max}, F_{fr,max}\right], \tag{57}$$

$$F^*_{flx} = 0.5(1-0.5)F^*_{ev}, \in \left[-F_{fl,max}, F_{fl,max}\right], \tag{58}$$

$$F^*_{rlx} = (1-0.5)(1-0.5)F^*_{ev}, \in \left[-F_{rl,max}, F_{rl,max}\right]. \tag{59}$$

3.2.3 Wheel

- **Ideal wheel**

For a rigid wheel, a simple direct inversion is enough, since it is non-causal. This means a division by the effective radius of the wheel will generate the reference torque required at the transmission. Thus,

$$T_{xyw}^{*} = r_w F_{xyx}^{*}. \tag{60}$$

- **Non-ideal wheel**

A much more complex inversion is required for this system, since not only is causal, many factors to control cannot be accurately measured in all situations. Therefore, many traction controllers have been proposed, such as the one used for the model, proposed by [5].

The controller used to limit the wheel slip is called Maximum Transmittable Torque Estimator, MTTE for short. It consists of computing a maximum torque the wheels can be provided to keep the slip at an optimal point in which the maximum force can be transmitted.

The working principle is greatly influenced by the ease in which many of the variables can be measured, for instance, the angular speed of the wheel can be measured easily, such as torque provided by the motor, but the linear speed of the vehicle is not so simple to accurately measure since it requires a variety of expensive, and not always reliable, sensors.

Therefore, [5] proposes the following control system to avoid the inversion of the μ-λ relation and the measurement of vehicle speed. According to (1) and (16), the friction force at the contact point between tire and ground can be expressed as

$$F_t = \frac{T}{r} - \frac{J_w \dot{v}_w}{r^2}. \tag{61}$$

where T and $\dot{v}_w$ will be measured from the system.

Once the friction force is estimated, the next step is to define the control input, this will be the torque, but it will require saturation in case slip becomes too high, this saturation is proposed to be

$$T_{max} = \left(1 + \frac{J_w}{\alpha M r^2}\right) F_t r - \frac{J_w}{\alpha M r}\left(F_g + F_w + F_r\right), \tag{62}$$

where α is the relaxation factor defined by

$$\alpha = \frac{\dot{v}_x}{\dot{v}_w} = \frac{(F_t - F_{res})/_M}{(T_{max} - F_t r)/_{J_w}}. \quad (63)$$

and is taken as 0.9 for the controller, to allow for the small slip to maximize the friction force.

3.2.4 Brake distributor

Before the transmission, the controller must decide how much braking torque is provided by the mechanical brake. Thus, a strategy block calculates how much torque the power train cannot provide and compensates for the lack of braking power by applying the required force. The expression is like that of the union, where

$$T^*_{xytrans} = (1 - k_{xy,brake)} T^*_{xyw}\,, \quad (64)$$

$$T^*_{xytrans} = k_{xy,brake} T^*_{xyw}\,, \quad (65)$$

where $k_{xy.brake}$ is computed by a complex system shown in Figure 3.2.2.

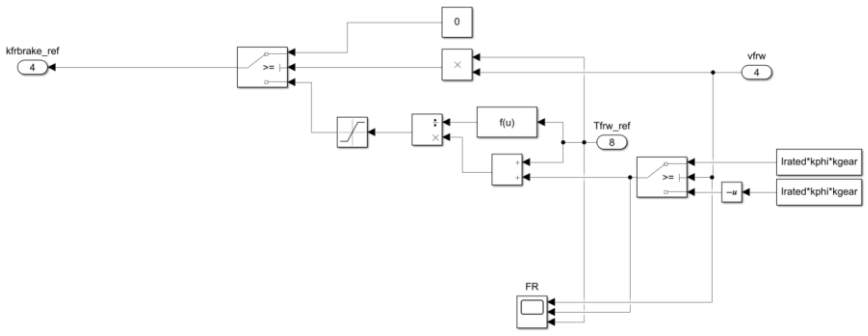

Figure 3.2.2: $k_{xy,brake}$ calculator system

3.2.5 Transmission

As well as the ideal wheel, the transmission is a simple conversion system, which can be directly inverted. Thus,

$$T^*_{xym} = k_{gear} T^*_{xytrans}. \quad (66)$$

3.2.6 DC motor

Once again, a causal system is encountered, not at the electromechanical coupling of the motor, which is represented as a conversion system, just as the transmission, by

$$I^*_{xya} = k\phi_a T^*_{xym}. \tag{67}$$

However, the electric conversion is causal, therefore, it requires a PI controller to properly invert the system. These PI controller parameters are computed as it was done for the chassis system, thus

$$K_P = \frac{\ln(9)}{t_{r,e}} L_a, \tag{68}$$

$$K_I = \frac{\ln(9)}{t_{r,e}} R_a. \tag{69}$$

The expression for the control system is represented by

$$U^*_{xya} = [K_P + K_I s]\left[I^*_{xya} - I_{xya}\right] - E_{xy}, \in [-400\ V, 400\ V] \tag{70}$$

Unlike the former proportional controller, this PI controller will have a saturation block at the exit. This paired to an integral controller means high levels of error if the output is saturated at any point, thus an anti-windup mechanism is implemented in which the output is compared and passed through a constant gain and subtracted from the integral part of the controller.

Once again, the behavior of the controller for different t_r values is given, see Figure 3.2.3.

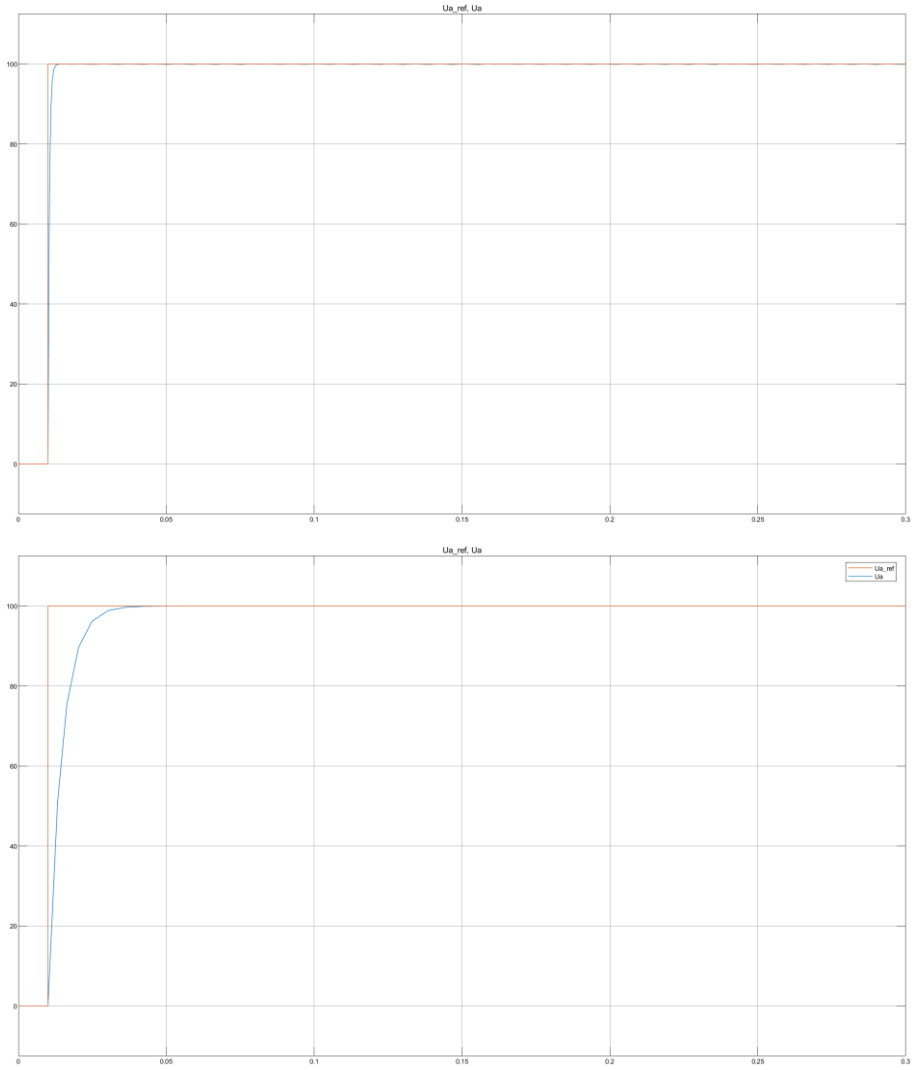

Figure 3.2.3: Voltage signal for a step input, (top) t_r=0.001 s and (bottom) t_r=0.01 s

3.2.7 DC/DC converter

At last, the DC/DC converter consists of a conversion system which takes the reference value from the motor and the current battery voltage output, and routed by the divisor, through the division and a limitation that more voltage cannot be provided than that of the battery, the duty cycle is generated. Thus,

$$\alpha_{xy}^{*} = \frac{U_{xya}^{*}}{V_{xya}}, \in [-1,1], \tag{71}$$

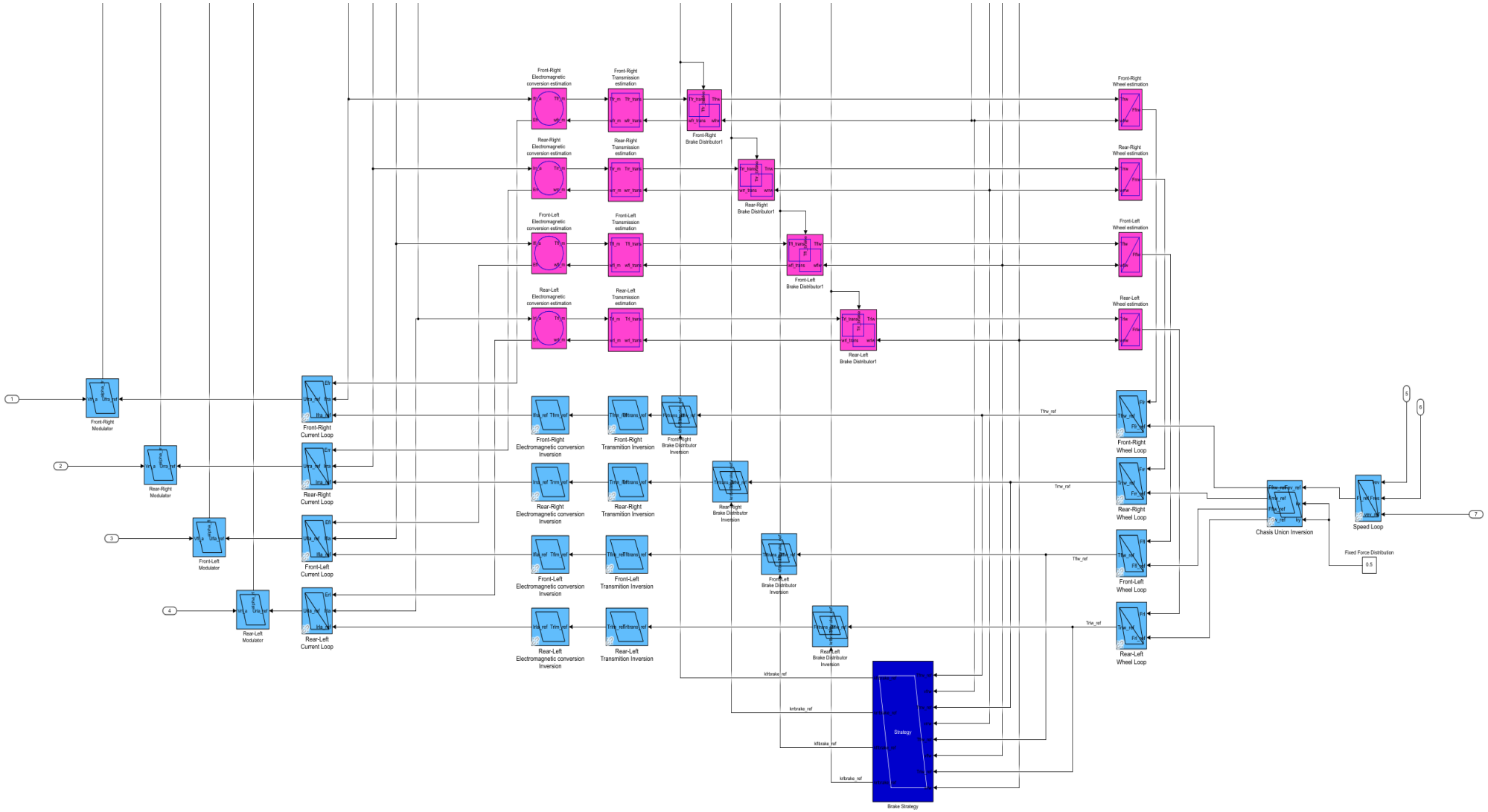

Figure 3.2.4: IBC model implemented in Simulink

4 SIMULATION

Once the theory behind modeling and control has been introduced, and the model and control systems themselves have been presented, the simulation results are provided for the two variations of the model developed: the rigid wheel model and the complex tire-road interaction model.

The simulation parameters are summarized in Table 4.1. bellow.

VEHICLE PARAMETERS		VALUE	UNITS
Vehicle Mass	m	1000	kg
Tire Effective Rolling Radius	r_w	0.26	m
Reduction Gear	k_{gear}	5	-
Air Density	ρ	1.22521	kg/m^3
Frag Coefficient	C_d	0.35	-
Frontal Area	A_f	2	m^2
Wheel Friction Coefficient	f_r	0.017	-
Gravity	g	9.81	m/s^2
Wheelbase	L	2	m
Center of gravity distance to the front axel	$Long_a$	1.2	m
Center of gravity distance to the front axel	$Long_b$	0.8	m
Center of gravity height	h_g	1	m
Axel inertia	J_w	0.5	kg·m2
Track	A_{ev}	1.65	m
BATTERY PARAMETERS		**VALUE**	**UNITS**
Battery constant voltage	E_0	3.7348	V
Equivalent resistance	R	0.09	Ω
Polarization voltage	K	0.00876	V
Exponential zone amplitude	A	0.468	V
Exponential zone time constant inverse	B	3.5294	As^{-1}
Rated voltage	V_{nom}	3.6	V
Rated cut-off voltage	V_{tall}	2.5	V
Rated capacity	Q_{nom}	1	Ah
ENVIRONMENT PARAMETERS		**VALUE**	**UNITS**
Inclination	Slope	0	º
Wind speed	v_w	0	m/s
MOTOR PARAMETERS		**VALUE**	**UNITS**
Rated power	P_{rated}	32000	W
Rated voltage	V_{rated}	400	V

Rated current	I_{rated}	89.5	I
Rated speed	rpm_{rated}	2840	rpm
Maximum speed	rpm_{max}	6000	Rpm
EMF constant	$K\phi_f$	1.2396	Vs/rad
Winding resistance	R_a	0,35	Ω
Winding inductance	L_a	6.50E-03	H
CONTROLLER PARAMETERS		**VALUE**	**UNITS**
Anti-windup gain	K_{aw}	10	-
Chassis time constant	t_{r_m}	0.1	s
Motor wiring time constant	t_{r_e}	0.01	s
BATTERY PACK PARAMETERS		**VALUE**	**UNITS**
Series cells	ns	160	Units
Parallel cells	np	100	Units

Table 4.1: Simulation parameters

4.1 FULL VEHICLE SIMULATION

As it has been introduced in the model description chapter, this variation is a simplification of the real road-wheel interaction, as the slip is not considered. This allows for multiple tests and evaluations, such as vehicle performance, battery consumption, range, or weight distribution analysis to name a few.

4.1.1 Acceleration and constant velocity

The first test that will be carried out is by giving the reference a step value of 15 m/s, this will generate an acceleration towards the reference value as shown in Figure 4.1.1. This acceleration is limited by one of two factors, either the road interaction does not allow for proper acceleration, or the motors themselves are caping the force to protect from overheating, the limitation is seen in Figure 4.1.2, as the referenced force is greater than the actual outputted force.

To verify the acceleration limitation Figure 4.1.3 is provided. Due to weight distribution, the front wheels cannot provide as much tractive effort as the rear wheels, losing on acceleration potential. Even though the front wheels are not producing the wanted force due to low contact with the ground, the main reason the acceleration is not higher is the limitation of the motors themselves as mention before, this can be seen as the reference force is capped at 6000 newtons due to a saturation block introduced in the controller.

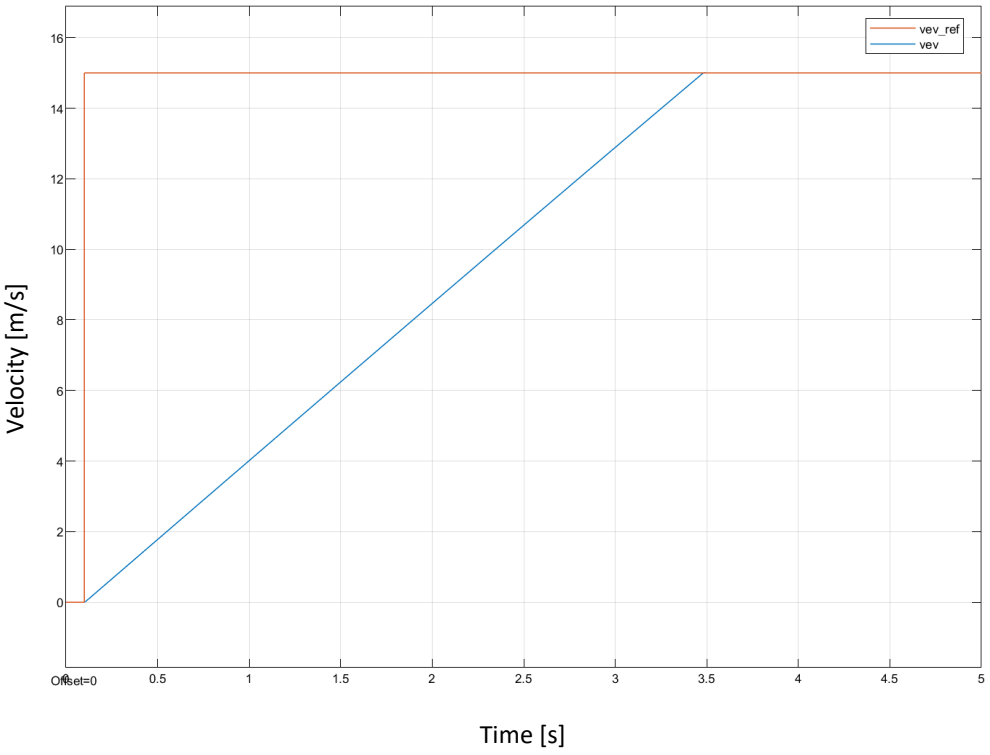

Figure 4.1.1: Reference speed and vehicle speed for a step input

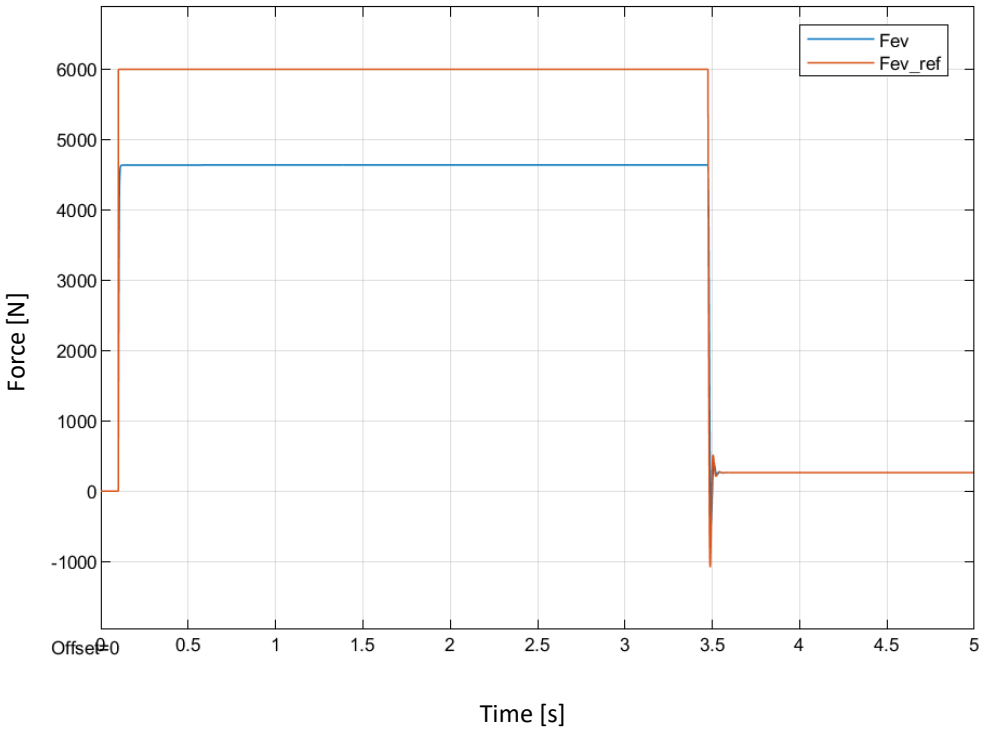

Figure 4.1.2: Force reference vs.outputed force

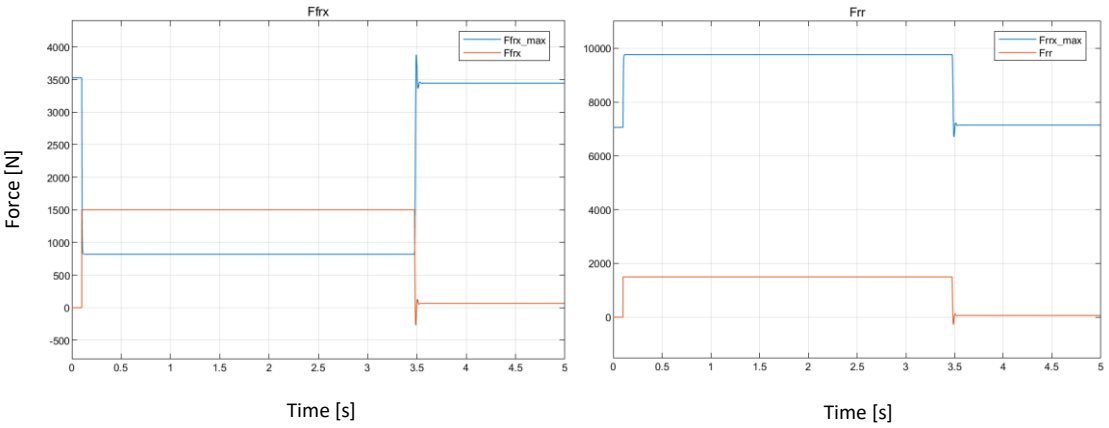

Figure 4.1.3: Maximum tractive effort vs tractive effort: (left) front wheels, (right) rear wheels

4.1.2 Deceleration

As acceleration has been tested, braking should be too. This will allow to see the proper behavior of the brake selector, which chooses the braking source to use. The speed profile is shown in Figure 4.1.4.

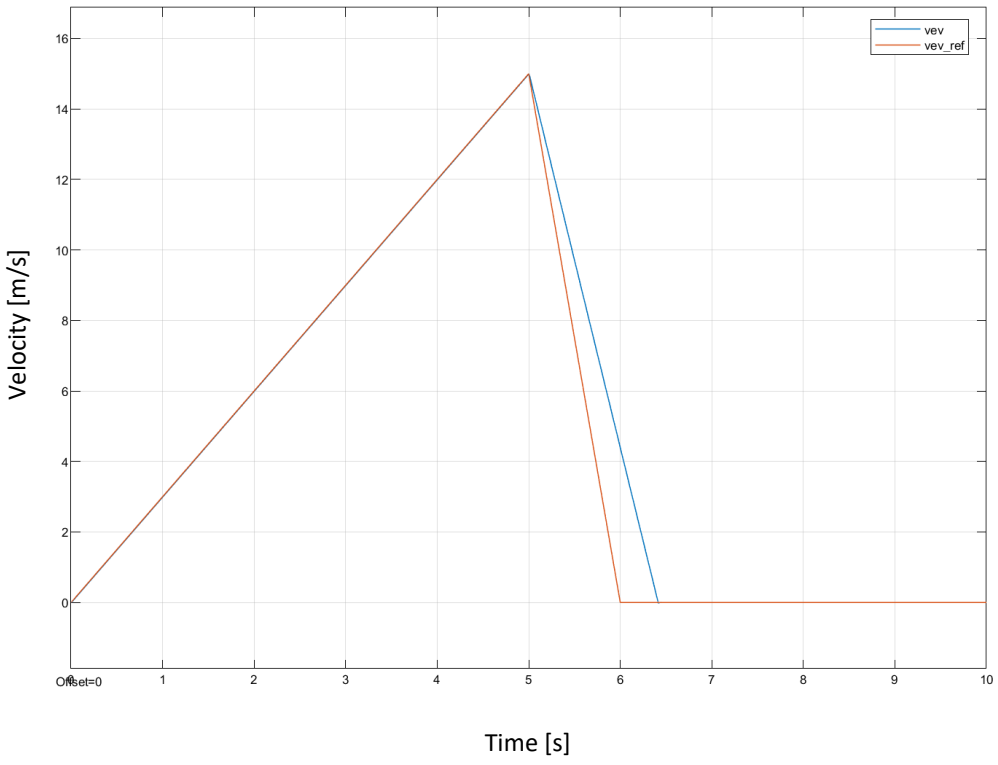

Figure 4.1.4: Speed profile, reference vs. Output

The steep braking requirement means the motor will not be able to produce the braking torque required, therefore, the mechanic brake will provide the extra torque, as shown in Figure 4.1.5, where it can be seen that for the front wheel a 60% of the braking is done with the mechanic brake. Again, braking capabilities are limited by the weight distribution, as the maximum tractive

effort limits the braking power, shown in Figure 4.1.6. At last, the energy regeneration can be seen in Figure 4.1.7, where the negative values of current represent an augment of state of charge of the battery.

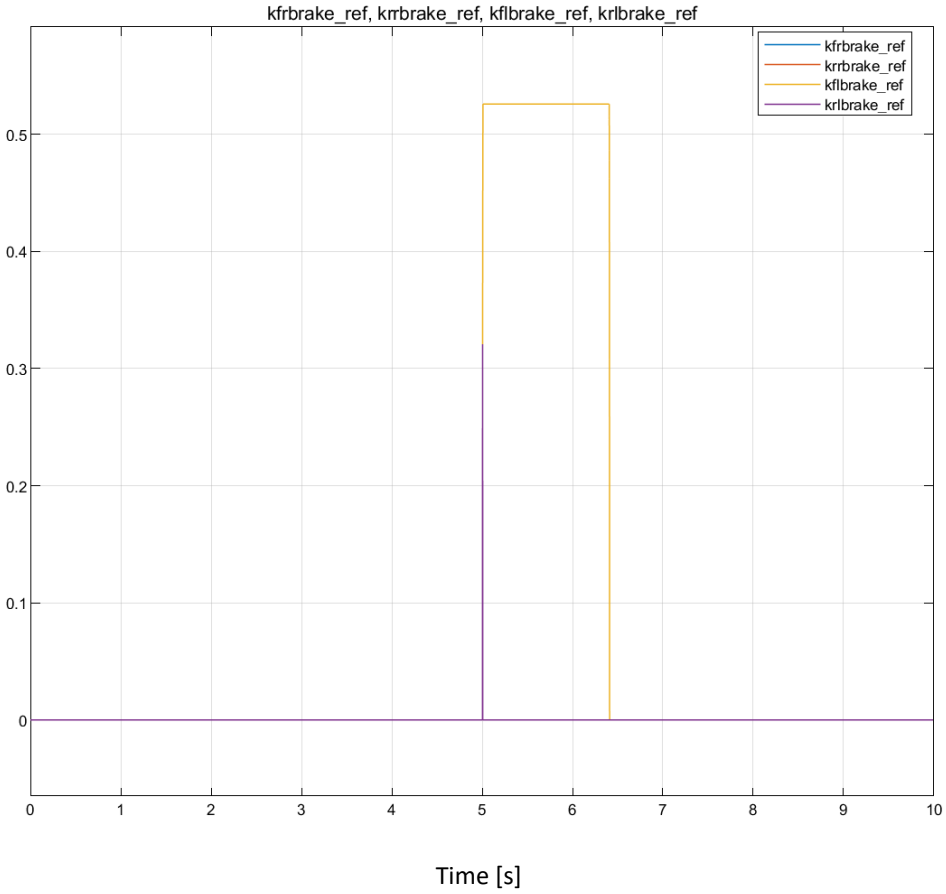

Figure 4.1.5: Percentage of braking effort provided by the mechanic brake

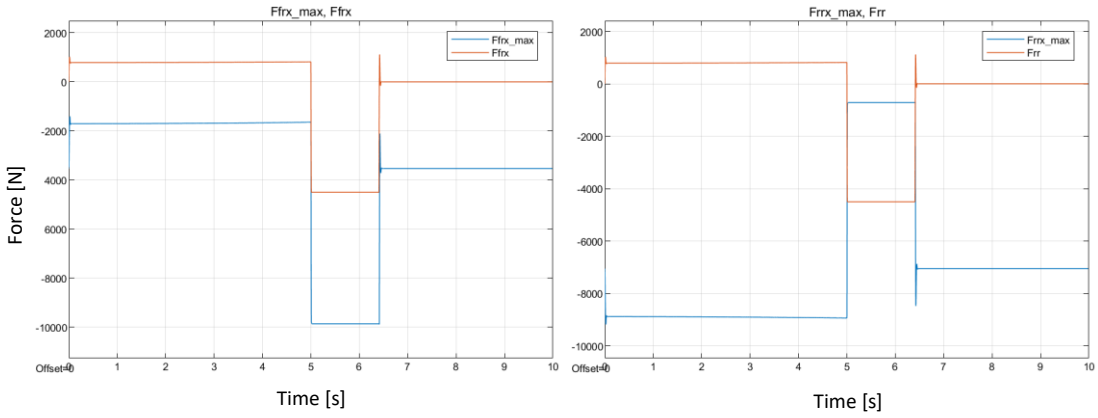

Figure 4.1.6: Maximum tractive effort vs tractive effort: (left) front wheels, (right) rear wheels

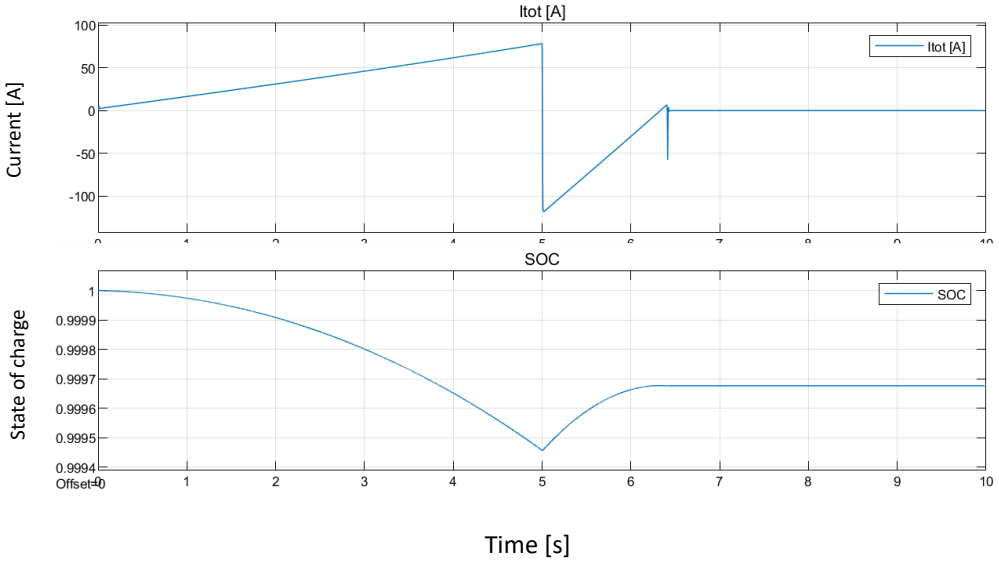

Figure 4.1.7: Battery current and SOC

4.1.3 Variable speed input

Finally, for more realistic testing of vehicle performance and behavior, speed cycles are used, such as the NEDC cycle, which emulates the speed profile a car follows while driving through a city and entering a highway. In Figure 4.1.8 the profile is displayed.

These profiles allow battery sizing to be more accurate, as the car can be simulated for long distances at realistic duty cycles. Therefore, many cell arrangements can be tested and determine optimal distribution. Since acceleration performance has been already tested before, only vehicle speed and battery parameters are to be analyzed.

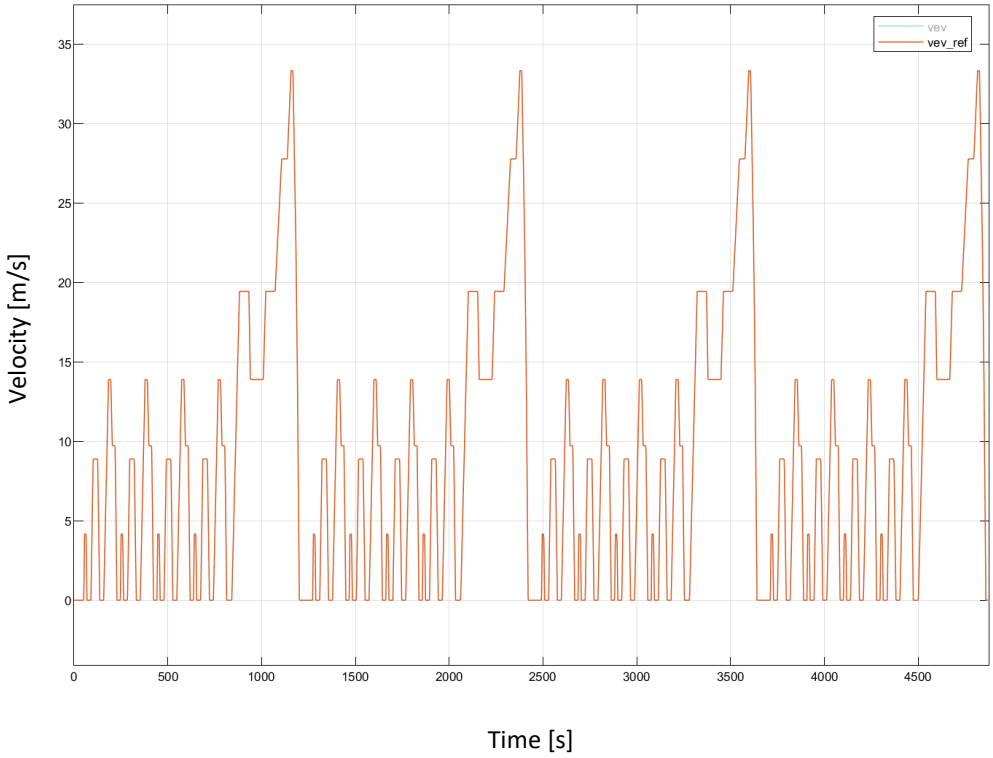

Figure 4.1.8: Reference speed profile of 4 NEDC cycle concatenated

Looking at the whole model as a black box, the first conclusion it can be extracted is the inability of the vehicle to follow the profile at high speeds as seen in Figure 4.1.9, which would mean that a more powerful motor should be tried, one with a higher rated voltage that does not cap the speed.

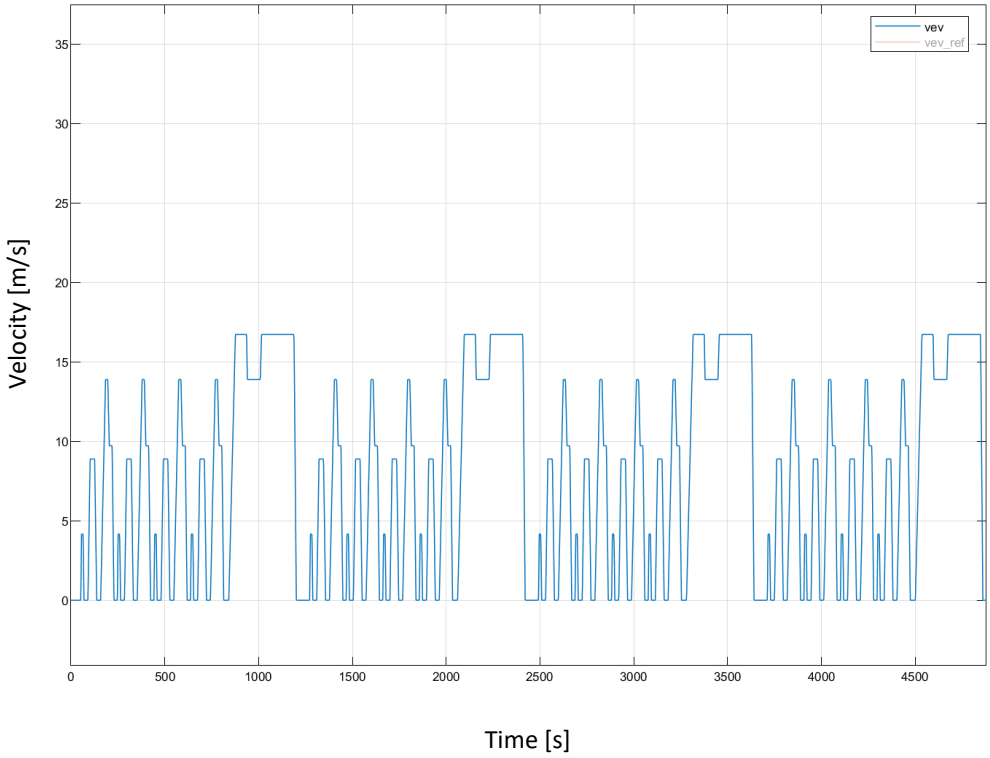

Figure 4.1.9: Output peed profile of 4 NEDC cycle concatenated

Next, the NEDC cycle simulation is useful to find out the required battery pack to withstand the desired range, as seen in Figure 4.1.10. For the tested cell arrangement, the SOC charge only drops to 96% and V_{bat} produces around 600 V, much more than the required by the motor, 400 V. Therefore, if the pack size is reduced to ns=120 and np=10 the behavior becomes as shown in Figure 4.1.11, where SOC drops to 60% by the end of the simulation. Furthermore, in both Figures 4.1.10 and 4.1.11, the effects of regenerative braking can be seen, as the current becomes negative the SOC rises slightly, extending the vehicle range.

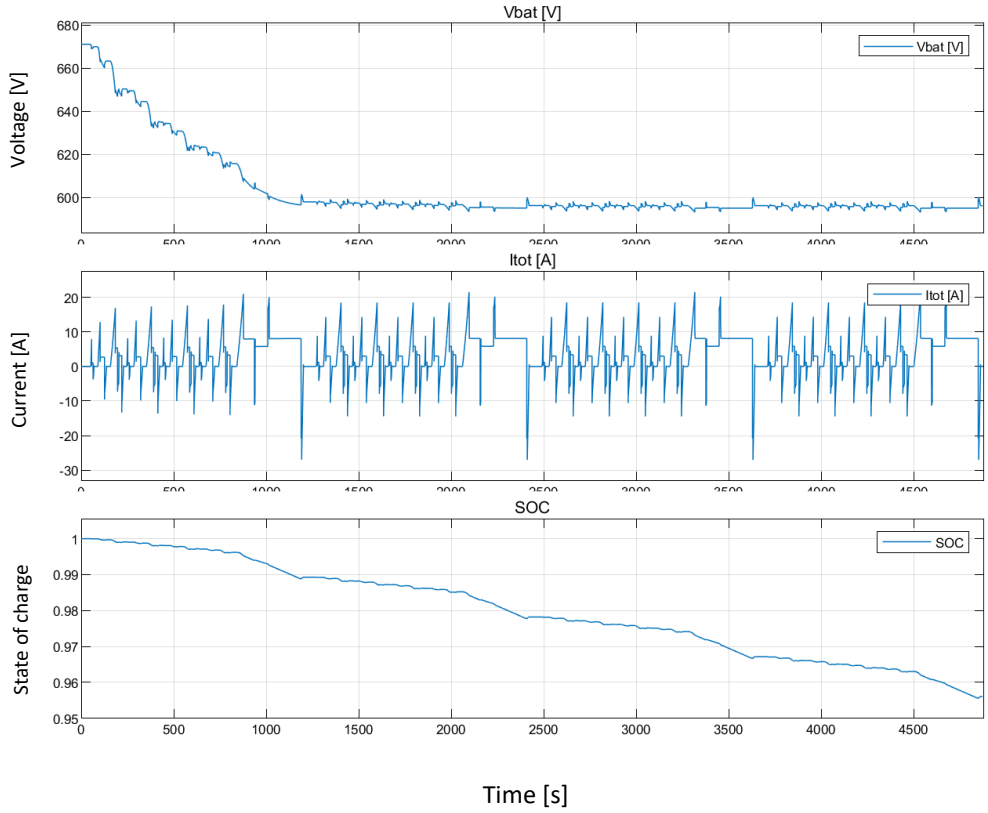

Figure 4.1.10: Battery evolution for a ns=160 and np=100 pack

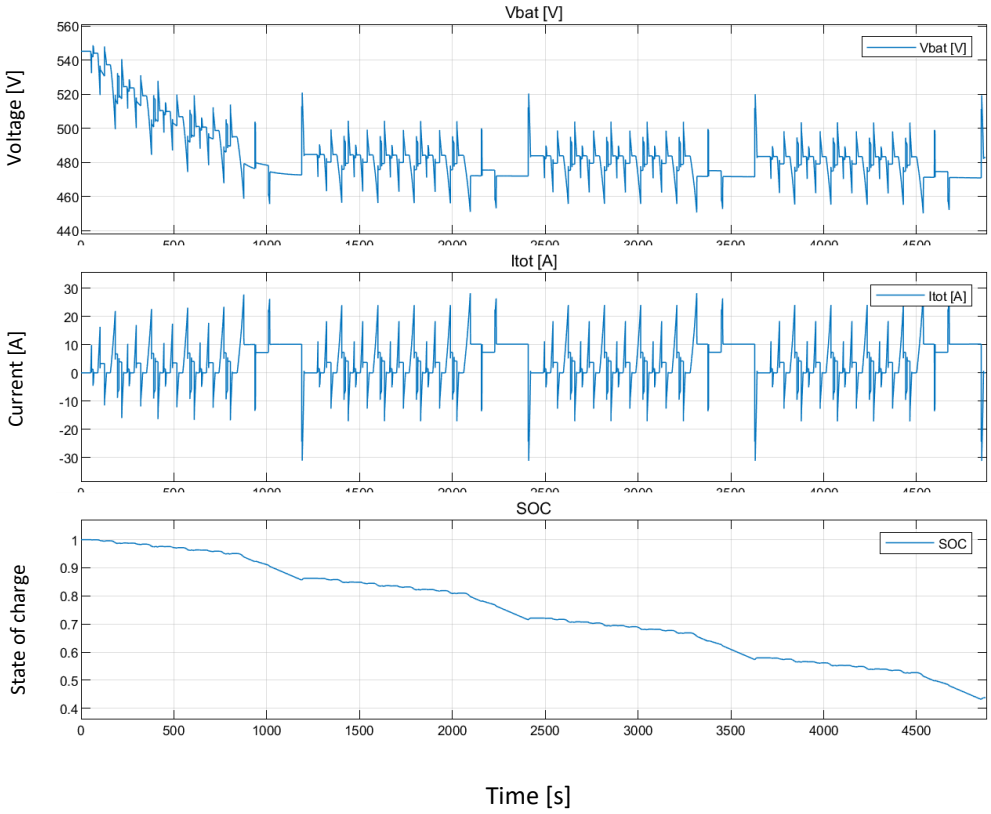

Figure 4.1.11: Battery evolution for a ns=120 and np=10 pack

4.2 TIRE-ROAD INTERACTION SIMULATION

As a real vehicle has a complex interaction between the ground it travels through and its tire, it is interesting to evaluate how the model behaves as the tire begins to slip.

4.2.1 Dry road acceleration

For the first simulation, a varying torque profile is taken, simulating the driver's desire of accelerating the vehicle.

As the vehicle starts in standstill some irregularities are presented at the beginning of the simulation. These irregularities begin with slip rising towards a value of 400, not displayed in Figure 4.2.1 as the desired zone of research, from 0 to 1, would not be appreciated.

After the irregularities associated with lower speeds, the system stabilizes and behaves properly, limiting the torque when needed to control the slip, as seen in Figure 4.2.1. It must be said, although the slip is perfectly controlled at around 20% producing the maximum tractive effort the vehicle is capable of, the acceleration ratio is kept under the desired value of 0.9, at around 0.2, as shown in Figure 4.2.3.

As for the input torque, in Figure 4.2.2 it can be seen how the controller limits the steps of the torque reference to provide the required force to prevent excessive slipping of the tire.

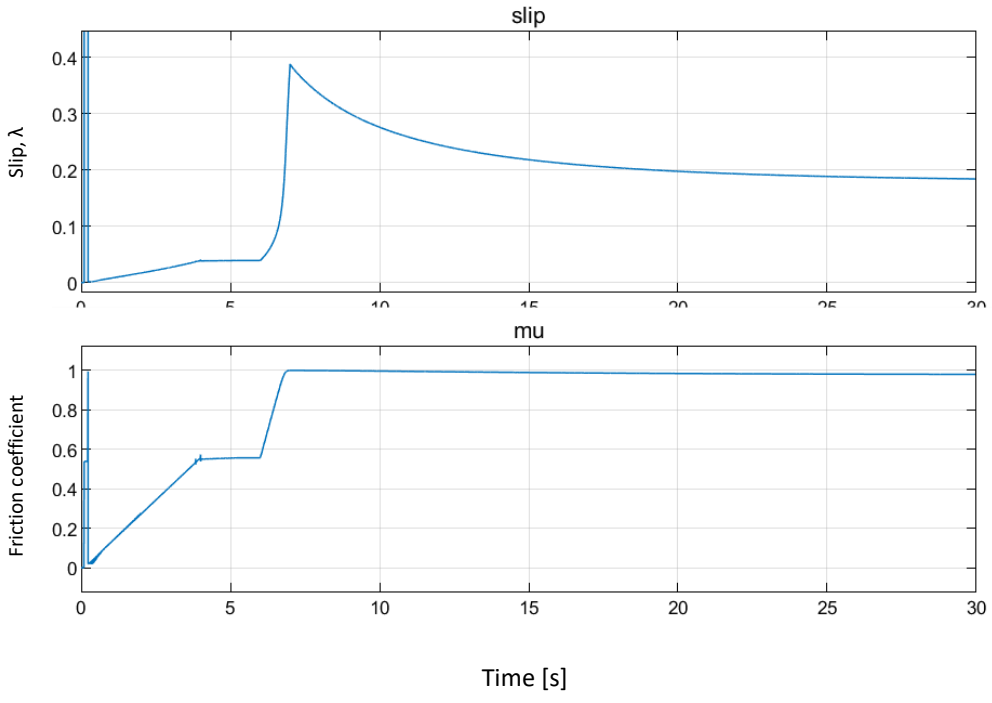

Figure 4.2.1: Slip (λ), top, and friction coefficient (μ), bottom, for a constant surface

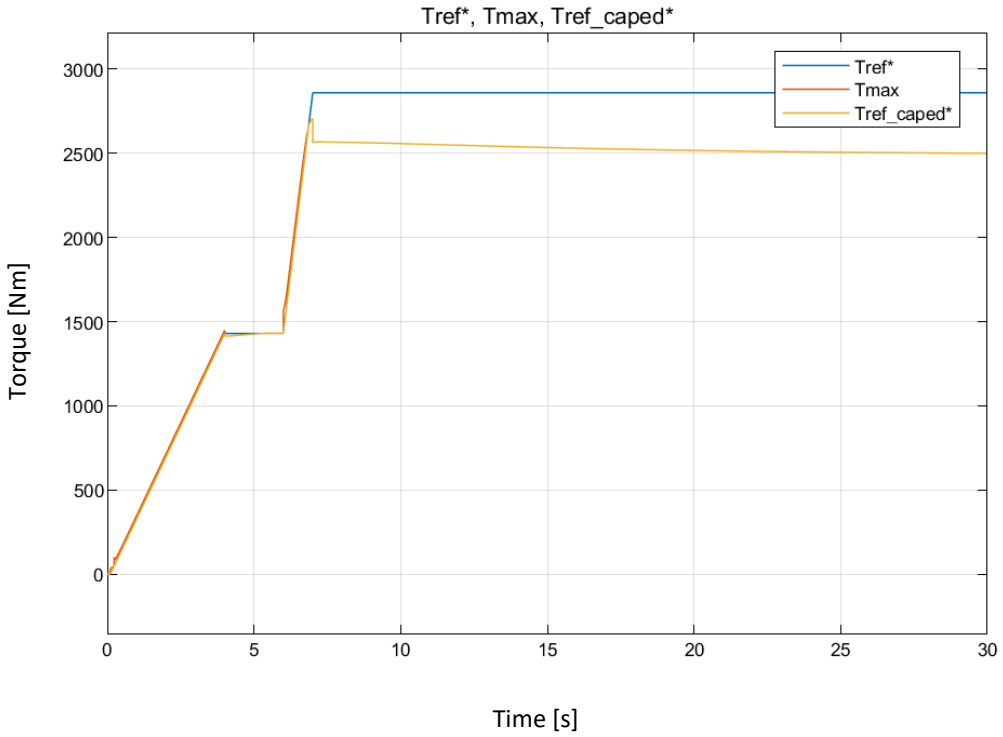

Figure 4.2.2: Reference toque, maximum torque and caped reference torque for a constant surface

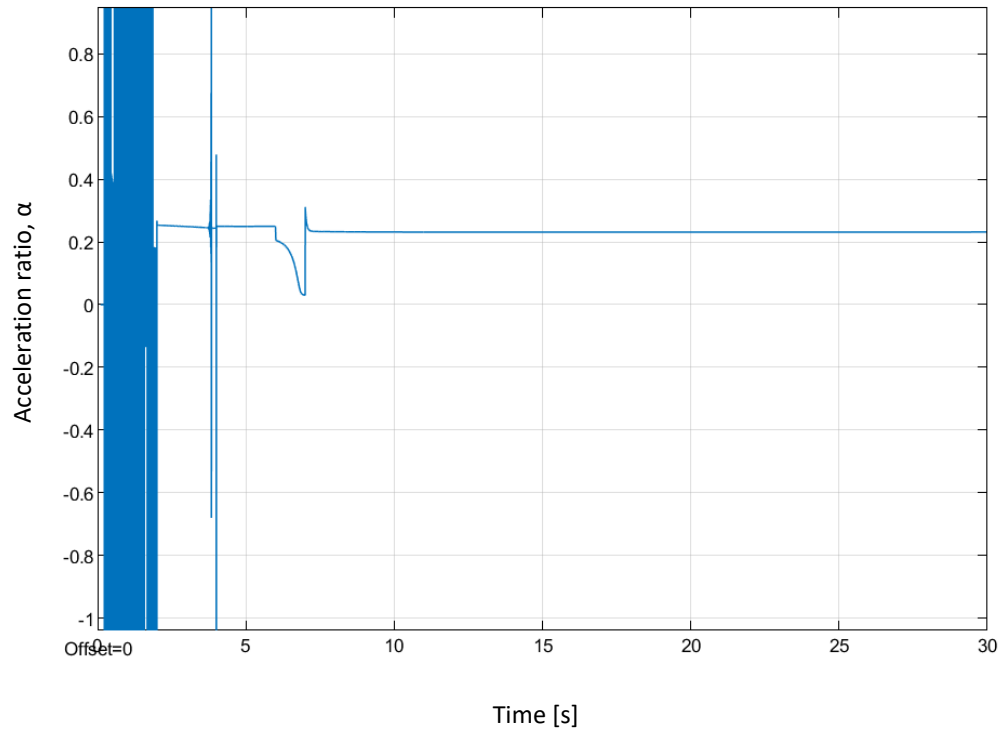

Figure 4.2.3: Ratio of acceleration for a constant surface

4.2.2 Dry road to wet road transition

As an extension of the previous simulation, a road transition phenomenon is introduced at 30 seconds to visualize the effects of increasing slip as the surface friction coefficient drops. In

Figure 4.2.4 it is seen how the slip increase as the vehicle enters a less grippy wet area but is later controlled at a value of 15 % to provide maximum friction as the surface changes.

As it was observed in the previous simulation, the torque reference is caped to prevent excessive slip when the friction coefficient drops, as represented in Figure 4.2.5.

And again, although the slip is controlled, the acceleration ratio is kept under the desired 0.9, although the slip is controlled at the desired value, as shown in Figure 4.2.6.

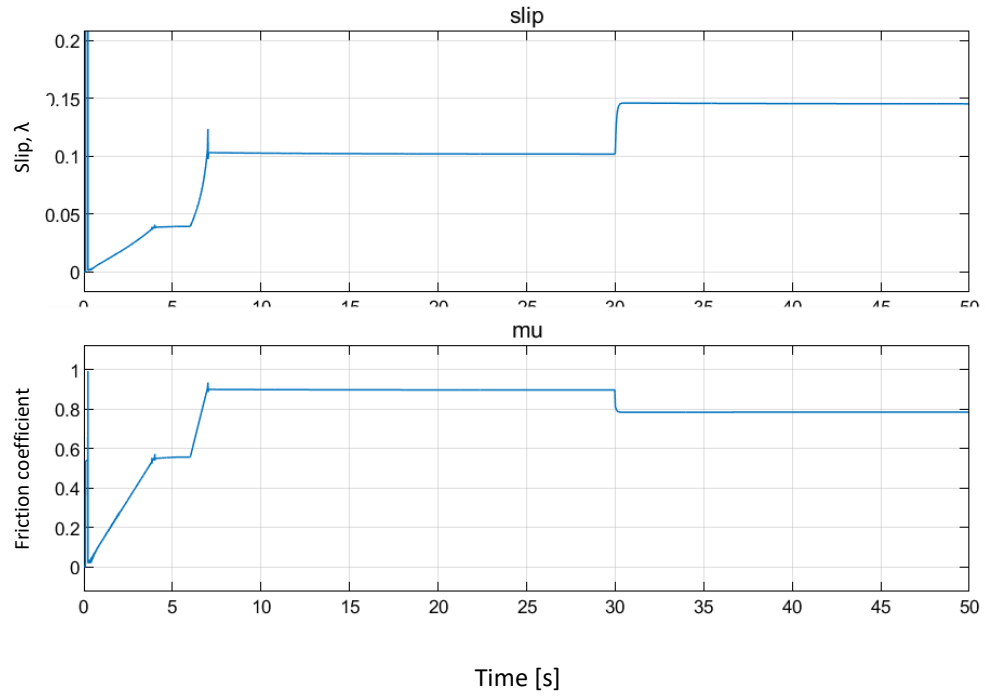

Figure 4.2.4: Slip (λ), top, and friction coefficient (μ), bottom, for a changing surface

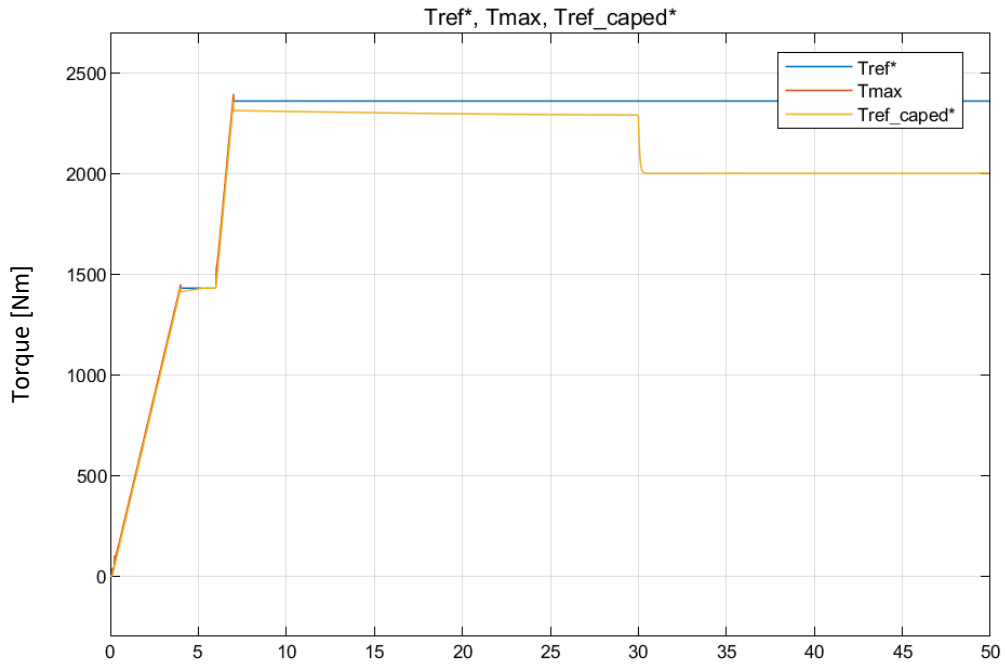

Time [s]

Figure 4.2.5: Reference toque, maximum torque and caped reference torque for a changing Surface

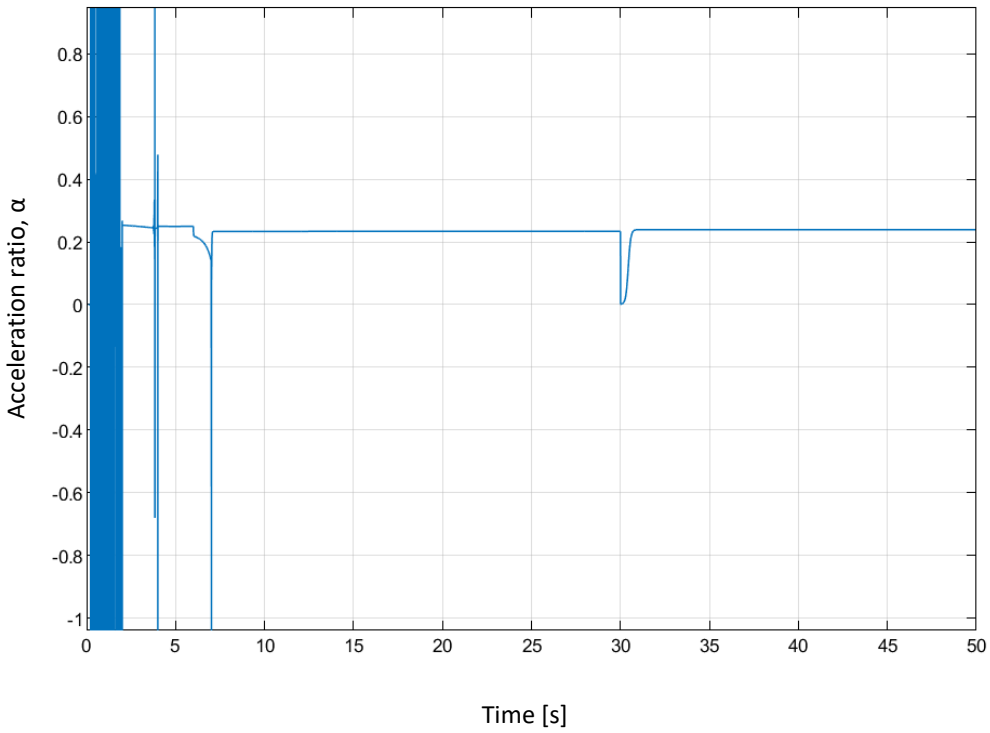

Figure 4.2.6: Ratio of acceleration for a changing surface

5 PLANNING AND BUDGET

5.1 PLANNING

For the project timeline, a Gantt diagram is provided in Figure 5.1.1, where the main activities realized in the project are plotted in time.

The project started on the 18th of February, as the first meeting with the project director was conducted, in it the main objectives where proposed and discussed. Once the objectives were defined the research for the project started.

First, the bibliography was consulted on vehicle dynamics, motor modeling, DC/DC converter theory, and battery modeling, creating a theoric basis for the model to be developed upon. As research was still underway, the model was stared, applying all the acquired knowledge from the literature consulted in previous weeks. Later, as the model development was concluding, investigation on control theory started, research on PID tuning, anti-windup mechanisms, and control performance was conducted, and once again, as the research advanced the control system model did too. Results analysis and validation were conducted afterward.

Once the ideal model was tested, and the report was started, the research for the complex tire-ground interaction was conducted. Once again, the research and development of the model were conducted at the same time. As the deadline closed in, the decision to drop the development of the control system was made and results were taken with the reduced model and the limited traction control.

Finally, the report was concluded adding the results of the reduced model and the project conclusions before the deadline.

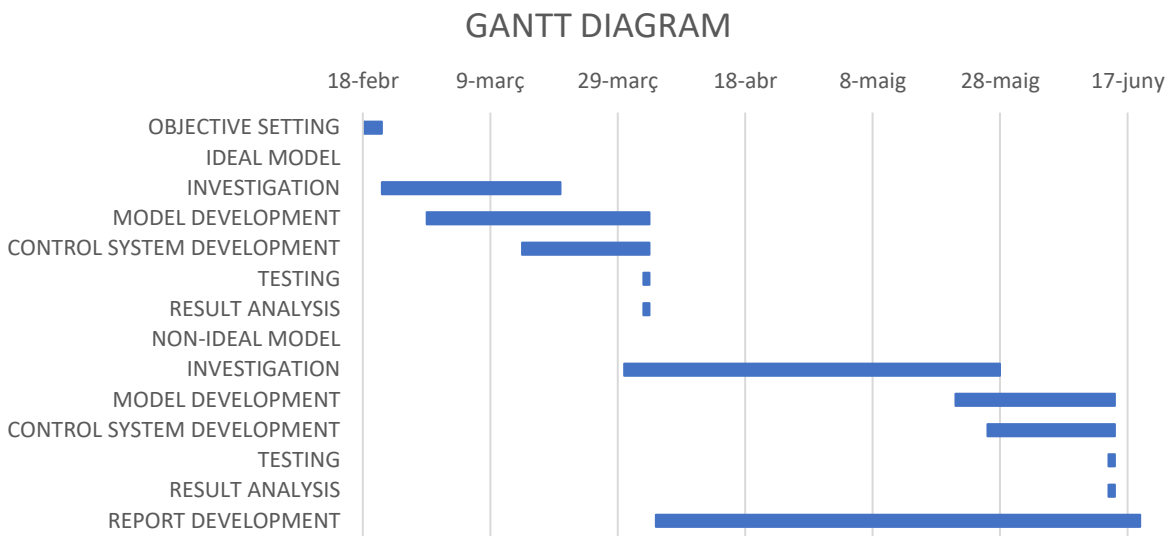

Figure 5.1.1: Gantt diagram of the project

5.2 BUDGET

In this chapter, the economic evaluation of the project is conducted. This evaluation is separated into human resources, software, hardware, and energy consumption.

First, for the estimation of human resources cost, assuming the net salary of a junior engineer being around 23€/h, and assuming a 3.5 hour a workday, from Monday through Friday, during 18 weeks, as shown in the Gantt diagram in Figure 5.1.1, the total ascends to 7245 €.

Second, the software is considered free, since the educational licenses for the software used, MatLab and Microsoft Office, are provided by the university.

Third, the hardware consists of only a personal computer, a Matebook pro 2018, listed at the time at 1500 €. Given the estimated lifespan of the computer at 6000 hours, and assuming 80% of the project duration requiring a computer, the total hardware cost becomes 62 €.

At last, the energy consumption of the project is computed as the hours of computer usage, 248 hours, times the average power consumption, 50 W, and the average cost of kWh of energy, 0.12 €/kWh. Therefore, the cost is 1.5 €.

A table is provided to summarize the cost breakdown in Table 5.1.

CONCEPT	UNITARY COST	UNITS	TOTAL
HUMAN RESOURCES			
Engineering hours	23 €/h	315 h	7245 €
HARDWARE			
Huawei Matebook Pro 2018	0.25 €/h	248 h	62 €
ENERGY CONSUMPTION			

Computer consumption	0.12 €/kWh	248 h	1.48 €
TOTAL			**7245.48 €**

Table 5.1: Economic evaluation

6 ENVIRONMENTAL IMPACT

In this chapter, an evaluation of the environmental impact of the project itself is presented alongside the environmental repercussions of the use of electric vehicles.

As the project objective was to develop a model and a control system for it without developing a prototype, the project itself does not pose a real impact other than the energy consumption of the computer. Thus, if the average consumption of the computer is around 50 W and the time the computer has been used is around 248 hours, the total energy consumption will be of 12,4 kWh. Taking the factor mix from 2019 of the company ENDESA ENERGÍA, S.A listed in [6] as 0.27 kg CO_2/kWh, the total carbon dioxide produced is 3.348 kg CO_2 for the whole project.

Moving past the emissions of running a computer, a brief analysis is made for the electrification of the vehicle fleet and its benefits and drawbacks considering environmental impact.

As the electric vehicle emissions when in movement are zero, unlike an internal combustion engine vehicle, the air quality of the area they are being used in is improved, an effect greatly appreciated in crowded urban areas.

That being said, electric vehicles cannot be considered zero-emission vehicles, since the recharge of the vehicle battery is done through the electric grid of the country it is charged in, and currently, this grid is composed in its majority by fossil fuel burning electric plants, represented by the factor mix in [6] not being zero. Therefore, the problem is moved from the location the car is driven through, to the location of the electric plant generating the energy. Furthermore, the manufacturing of the vehicle generates carbon dioxide and many more pollutants associated with the mining of materials required, manufacturing process, and assembly of parts. At last, the lithium-ion battery packs used for most electric vehicles have a great environmental impact as its production is highly pollutant.

In conclusion, the electric vehicle has the benefit of not polluting the environment it drives through, like crowded cities, improving the air quality of the area, but it does not mean the vehicle is zero emissions, as it has been shown the emissions are generated anyway. Therefore, development on renewable electric plants must be done to reduce the impact of production and recharging each vehicle, bringing down the total emissions.

7 CONCLUSIONS

First, research on the dynamic behavior of the vehicle has been performed, which allowed modeling the environment interaction with the vehicle through the chassis and tire. Furthermore, analysis of the motor, battery, and other subcomponents dynamics and behavior, allowed for a full vehicle model capable of analyzing the interaction between them and the environment earlier described.

As it has been mentioned throughout the project, two models had to be developed, one for the whole vehicle with a simple wheel, and a reduced model with the complex tire-ground interaction. Although the later one was not possible to implement directly into the whole electric vehicle model, due to simulation problems induced by the controller implementation, it was still possible to extract value out of it.

For the control system, the conclusions are more complex. As the controller for the whole vehicle model worked as expected, the reduced model for the complex tire-road interaction had some problems. These problems involved the interaction between controllers and poor performance at slow speeds, non-steady-state situations, and following decelerating profiles. All these cases would make the simulation to go unstable or spark an error message, therefore invalidating the simulation. However, some simulations could be performed and provided promising results, as the vehicle slip was controlled at optimal values.

Overall, the objectives set at the start of the project have been met, except for the full traction control which is limited to specific situations.

FUTURE WORK

As the project comes to an end, a reflection is done on the future work it could be done to further develop it.

In terms of research, a more robust definition of road-tire interaction could be found, since the proposed by Pacejka and Burckhardt presents problems with speeds near 0 and non-steady-state situations generate great error and oscillation. Therefore, a solution could be found in which the complex wheel is implemented into the whole vehicle model without problems with its controller.

As for the model, a few changes could be made to improve the value it has to the industry. Right now, induction machines and permanent magnets brushless machines are dominating the

market, thus, it would be interesting to test the vehicle performance with this kind of motor, although, it would require a change in the control system, augmenting its complexity. As for the reduced model, the lateral slip should be considered, adding a layer of complexity to the tire-road interaction.

Furthermore, the mainline of future work is the actual controller, regarding traction control. Developing a proper traction control system in which low-speed situations or transitioning from acceleration to braking do not pose a problem should be of utmost priority, as a control system cannot be tested in a real vehicle if it will not allow it to brake or alter speed as desired.

8 BIBLIOGRAPHY

[1] M. Ehsani, Y. Gao, S. E. Gay and A. Emadi, Modern electric, hybrid electric, and fuel cells vehicles: fundamentals, theory, and design, 2005.

[2] H. B. Pacejka, Tyre and vehicle dynamics, 2002.

[3] A. Bouscayrol, A. Bruyère and P. Delarue, Teaching drive control using Energetic Macroscopic Representation, 2007.

[4] O. Tremblay, L. A. Dessaint and A.-I. Dekkiche, A generic battery model for the dynamic simulation of hybrid electric vehicle, 2007.

[5] D. Yin, S. Oh and Y. Hori, A novel traction control for EV based on maximum transmissible torque estimation, 2009.

[6] g. d. E. Ministerio para la transición ecológica y el reto demográfico, Factores de emisión: registro de huella de carbono, compensación y proyectos de absorción de dióxodo de carbono, 2020.